ADVANCING EARTH AND SPACE SCIENCE

Earth's Future

RESEARCH ARTICLE
10.1029/2022EF003009

Diverging Trends in Rain-On-Snow Over High Mountain Asia

Fadji Z. Maina[1,2] **and Sujay V. Kumar**[1]

[1]Hydrological Sciences Laboratory, NASA Goddard Space Flight Center, Greenbelt, MD, USA, [2]Goddard Earth Sciences Technology and Research Studies and Investigations, University of Maryland, Baltimore County, Baltimore, MD, USA

Key Points:

- In the Indus, rain-on-snow (ROS) represents more than 5% of the annual precipitation and has an increasing trend
- In the Ganges-Brahmaputra, ROS which represents more than 10% of the annual precipitation is decreasing
- In the Amu Darya, Syr Darya, and Ili, ROS constitutes 5%–10% of the annual precipitation and has a bidirectional trend

Correspondence to:
F. Z. Maina,
fadjizaouna.maina@nasa.gov

Citation:
Maina, F. Z., & Kumar, S. V. (2023). Diverging trends in rain-on-snow over High Mountain Asia. *Earth's Future*, *11*, e2022EF003009. https://doi.org/10.1029/2022EF003009

Received 27 JUN 2022
Accepted 8 FEB 2023

Abstract Rain-on-snow (ROS) over snow-dominated regions such as High Mountain Asia (HMA) modulates snowmelt and runoff and is key contributor in influencing water availability and hazards (e.g., floods and landslides). We studied the trends in ROS in HMA over the past two decades from 2001 to 2018 using the land surface model Noah-MP driven by an ensemble precipitation data set. Our results show that changes in precipitation phase and rainfall are altering ROS. Because of the strong physical heterogeneity and atmospheric dynamics of HMA, ROS characteristics and trends are region-dependent and ROS occurs predominantly over the Indus, Ganges-Brahmaputra, and northwestern basins. In the Indus, ROS representing ~5% of the annual precipitation and ~20% of the annual snowmelt, has an increasing trend. This is contrary to the Ganges-Brahmaputra characterized by decreasing ROS trends, where it represents ~11% of the annual precipitation and ~60% of the annual snowmelt. In the northwestern basins, ROS has bidirectional trends due to elevation patterns and trends in rainfall, and it constitutes ~5 to ~10% of the annual precipitation. Increasing trends in ROS over Indus contribute to reducing the snowpack in late summer, with concerns of reduced water availability and increased groundwater exploitation. Similarly, because of its high amount and contribution to snowmelt, the decreasing ROS trends in the Ganges-Brahmaputra will have consequences of decreased recharge from the headwaters and exacerbated use of groundwater unless increasing trends in rainfall compensate for the decreasing snowmelt. These results provide new insights on ROS-driven changes in the hydrological cycle over HMA.

1. Introduction

High Mountain Asia (HMA), a region that includes the Tibetan Plateau and the Himalayan, Karakoram, Pamir, Hindu Kush, and Tien Shan mountains, represents the headwaters of Asia's most prominent hydrologic basins, which feed billions of people (Immerzeel et al., 2010; Pritchard, 2019; Qiu, 2008). HMA is subject to warming at an alarming rate (Immerzeel et al., 2010), with the increases in temperature leading to a shift in the precipitation phase and more precipitation falling as rainfall instead of snowfall (Y. Li et al., 2020; Smith & Bookhagen, 2018). In addition, precipitation rates are increasing in many regions of HMA (Maina, Kumar, Albergel, & Mahanama, 2022; Maina, Kumar, Dollan, & Maggioni, 2022). These patterns could cause rain-on-snow (ROS) (McCabe et al., 2007; Ye et al., 2008). With ongoing global warming, ROS is becoming more frequent in mountainous regions around the world with dramatic consequences on downstream hydrology (Freudiger et al., 2014; McCabe et al., 2007; Musselman et al., 2018). Moreover, the impacts of ROS are projected to become worse in the future (Beniston & Stoffel, 2016; Chegwidden et al., 2020; López-Moreno et al., 2021; Morán-Tejeda et al., 2016; Ohba & Kawase, 2020; Ye et al., 2008). Although the risks of ROS in other regions around the world have been documented (Cohen et al., 2015; Garvelmann et al., 2014; D. Li et al., 2019; Musselman et al., 2018; Singh et al., 1997), such studies investigating ROS in their impacts on runoff over HMA are lacking, to the best of our knowledge. As HMA hosts the largest reservoirs of freshwater outside the polar zone, quantifying changes in ROS is particularly important for water resources and hazard mitigation applications.

ROS has attracted the attention of hydrologists in the past decades because of its increasing occurrences and consequences in many parts of the world. Recent publications have qualified ROS as one of the 23 unsolved hydrological problems in the context of complex water management (Blöschl et al., 2019). Although not frequent, ROS has significant impacts on hydrology. It exacerbates the melting of snow, which warms the soil and accelerates the decrease of the snowpack. Hydrological processes are complex after ROS because the hydrodynamics of ROS depend on many factors (Cohen et al., 2015; Groisman et al., 2005; J. Putkonen & Roe, 2003). For instance, the effects of ROS depend on the characteristics of the snowpack itself. ROS on a snowpack that has not started to melt only penetrates its first centimeters, whereas on a melting snowpack, ROS quickly penetrates the entire snowpack and accelerates its melting (Groisman et al., 2005). ROS could

also change the timing of snow dynamics. For example, in the case of a small snowpack, ROS shifts the timing of the snowmelt and makes the snowpack last for a shorter duration. The early snowmelt and the resulting smaller snowpack will decrease soil moisture in summer, which could lead to drought (Cohen et al., 2015). In addition, the impacts of ROS depend on the season. In fall and winter, ROS impacts soil properties and snow properties prior to the snowmelt season, while in spring, ROS amplifies snowmelt, runoff, and flood risk. Also, ROS constrains surface soil temperatures close to 0°C in regions that would otherwise be well below freezing (Putkonen & Roe, 2003). ROS consequences are, therefore, complex and include floods, snow avalanches, soil erosion, and sediments transportation (Bieniek et al., 2018; Crawford et al., 2020; Marks et al., 1998; Singh et al., 1997; Stimberis & Rubin, 2011) which can lead to landslides and geomorphological changes (Harr, 1981). On a longer timescale, ROS could lead to drought and impact vegetation growth because it changes the soil temperature (Putkonen et al., 2009; Putkonen & Roe, 2003). By affecting the latent heat fluxes, ROS is also susceptible to changing the energy budget and therefore the interactions between the land and the atmosphere (Westermann et al., 2011) and subsequently the energy of snowmelt processes. Therefore, a better understanding of ROS is critical to assessing the impacts of a changing climate because ROS has the potential to exacerbate and/or accelerate the impacts of climate change and its effects should be accounted for in mitigation strategies.

As net shortwave and longwave radiation and the turbulent fluxes of sensible and latent heat, very important to snowmelt processes, are highly impacted by the topography and the vegetation (Garvelmann et al., 2014, 2015; Pohl et al., 2006; Wayand et al., 2015), ROS effects are region-dependent. Cohen et al. (2015) studied ROS in the northern hemisphere and concluded that ROS mainly occurs in western Eurasia, the higher elevations of western North America, the northeastern United States, and southeastern Canada. ROS has also been studied in Asia (Ohba & Kawase, 2020; Whitaker & Sugiyama, 2005; Yang et al., 2022), Europe (Garvelmann et al., 2015; Pall et al., 2019; Rössler et al., 2014; Ulbrich & Fink, 1995), Artic (Rennert et al., 2009), Canada (Loukas et al., 2000; Trubilowicz & Moore, 2017), and the United States where ROS events have generated some of the costliest natural disasters of the country (Bieniek et al., 2018; Jeong & Sushama, 2018; Leathers et al., 1998; McCabe et al., 2007; Musselman et al., 2018; Pradhanang et al., 2013). In central Europe, for example, studies have shown that 20%–80% of peak flows are associated with ROS (Merz & Blöschl, 2003; Nied et al., 2014; Sui & Koehler, 2001; Tarasova et al., 2020).

Despite the socioeconomic impacts of ROS, little is known about how ROS varies in time, spatial extent, and intensity across HMA's mountainous areas. Because of its hydrological impacts, ROS is relevant for water resources management and flood forecasting (Freudiger et al., 2014; McCabe et al., 2007). However, the quantification of ROS in mountainous and remote regions could be difficult due to the lack of ground observations and the uncertainties associated with the estimation of precipitation (Palazzi et al., 2013; Yoon et al., 2019; You et al., 2015). Changes in air temperature are also difficult to estimate in these areas because of their orographic patterns (Lalande et al., 2021).

In this study, we assess the changes of ROS in HMA over the two past decades from 2001 to 2018 based on land surface model simulations informed by high quality precipitation inputs and remote sensing information on snow conditions. Specifically, the land surface model Noah-MultiParameterization (Noah-MP, Niu et al., 2011) is driven with an ensemble precipitation product (Maina, Kumar, Dollan, & Maggioni, 2022) generated using the best available gridded precipitation products that includes the Integrated Multi-satellitE Retrievals for Global Precipitation Measurement IMERG (Huffman et al., 2015), the Climate Hazards group Infrared Precipitation with Stations CHIRPS (Funk et al., 2015), and the ECMWF Reanalysis ERA5 (Hersbach et al., 2020). These precipitation products were found to better represent the precipitation averages and trends in HMA (Maina, Kumar, Dollan, & Maggioni, 2022). The land surface model Noah-MP allows for a physical representation of the key HMA's dynamics such as snow dynamics, vegetation dynamics, and hydrodynamics by physically solving the water and energy budgets. Noah-MP has successfully been used to study water budgets in HMA (Ahmad et al., 2022; Xue et al., 2019, 2022; Yoon et al., 2019). To reduce the uncertainties in simulations of snow, a remote sensing-based reconstructed snow water equivalent (SWE) data developed by Kraaijenbrink et al. (2021) is assimilated within the land surface model integrations. The model simulations are then employed to:

- Quantify ROS days and amounts in HMA and their trends
- Quantify the contributions of ROS to the snowmelt and the water available for runoff in HMA

10.1029/2022EF003009

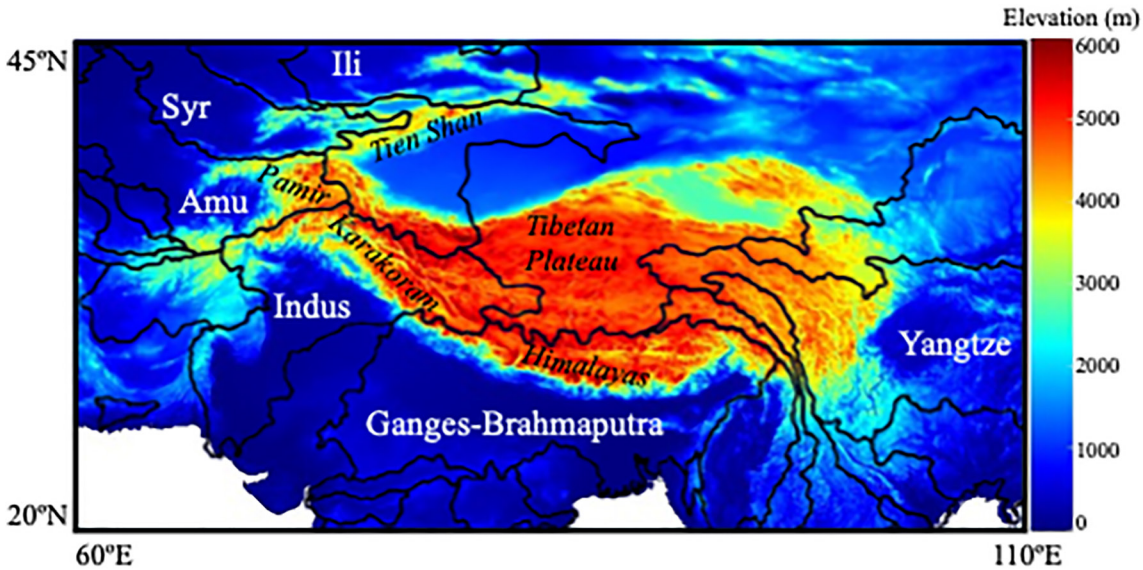

Figure 1. Map of High Mountain Asia: elevation, major hydrological basins, and mountains.

2. Study Area and Methods

2.1. Study Area: High Mountain Asia (HMA)

HMA as defined in this study extends from approximately 20°N to 46°N, and 60°E to 111°E and includes the Tibetan plateau and other mountains such as the Himalayas, Hindu Kush, and Tien Shan (Figure 1). These mountains represent the headwaters of Asia's major rivers such as the Yangtze, the Ganges, the Brahmaputra, and the Indus (Viviroli et al., 2007) which flow through many countries (e.g., China, Myanmar, Bhutan, Nepal, Bangladesh, India, Pakistan, Afghanistan, and Kyrgyzstan). The economy of these countries largely depends on HMA water towers, a lifeline to more than a billion people living in its hydrologic basins (Yangtze, Si, Song Hong, Irrawaddy, Hwang Ho, Ganges-Brahmaputra-Brahmaputra, Indus, Tarim, Ili, Amu Darya, and Syr Darya, see Figure 1). HMA is characterized by sharp variations in topography with elevation varying from sea level to the world's highest point at Mount Everest (8,848 m). This complex orography along with strong heterogeneities in land cover and harsh climatology makes the high elevation areas of the HMA a hostile environment not easily accessible. As a result, ground measurements are rare, not reliable, and very sparse in both time and space making remote sensing data the only available data to study the hydrology of the region.

2.2. Methods

2.2.1. Model Set-Up

We use the Noah-MP land surface model version 4.0.1. to simulate land surface processes including snow accumulation and melt (Niu et al., 2011). Noah-MP allows simulations with various options compared to the previous versions of the model Noah and includes the choice of multiple options for the snowpack, vegetation, infiltration, and runoff physics computations (Niu et al., 2011). The Noah-MP model simulations are driven with an ensemble precipitation data set generated by Maina, Kumar, Dollan, and Maggioni (2022) using a localized probability matched method (Clark, 2017) with three gridded precipitation products (IMERG, CHIRPS, and ERA5) while the other meteorological forcing (temperature, shortwave, and longwave radiation, wind speed, relative humidity, etc.) are generated by downscaling ERA5 following Xue et al. (2019, 2022). HMA precipitation is highly uncertain due to the lack of reliable ground measurements. Consequently, gridded precipitation products are not consistent across the region. The ensemble precipitation product is specifically developed to overcome the inconsistencies between different precipitation data and to have the best product capturing the precipitation dynamics in the region. In addition, we used ERA5 for other meteorological forcings because the trends in ERA5 variables (e.g., temperature) are consistent with observed warming in HMA (Immerzeel et al., 2010). The model simulations employ landcover data derived from the Moderate Resolution Imaging Spectroradiometer (MODIS;

Friedl & Sulla-Menashe, 2019), soil types derived from the International Soil Reference and Information Center (ISRIC—World Soil Information, 2022) and topographic information from MERIT-DEM (Multi Error Removed Improved Terrain Digital Elevation Model; Yamazaki et al., 2017).

The Noah-MP model is run at a spatial resolution of 5 km and a temporal resolution of 15 min during a period of 2001–2018. Although this time frame could be considered relatively short for long term trends analysis, we selected this period based on the common availability of datasets we used (e.g., remote sensing such as MODIS and precipitation data such as IMERG). To generate the initial conditions for the model simulations, we however, opt to run the model twice for a longer period 1990 to 2018. To better assess the changes in ROS in HMA, reliable estimates of SWE are necessary. However, because of the lack of ground measurements, accurate estimations of SWE are difficult to obtain, and the majority of the available SWE estimates relies on reanalyzes. In this study, we use the SWE reconstruction developed by Kraaijenbrink et al. (2021), which employs a temperature index melt model (Hock, 2003) along with ERA5 forcing, and MODIS snow cover (Hall et al., 2006) to develop multidecadal estimates of SWE. More details about the model calibration and evaluation can be found in Kraaijenbrink et al. (2021). This SWE product is then assimilated to constrain the Noah-MP simulations. Note that only the SWE is assimilated to the model, the snow dynamics and melt estimation is performed by Noah-MP, which includes a multi-layer snowpack formulation that explicitly accounts for liquid water storage, melt, refreeze, and sublimation processes.

To assimilate the SWE reconstruction data, we use the 1-dimensional Ensemble Kalman Filter algorithm (EnKF; Reichle et al., 2002). EnKF is an optimal sequential data assimilation method for nonlinear dynamics and has been widely used to assimilate remotely sensed variables into the land surface model Noah-MP (Kumar et al., 2014; Lahmers et al., 2022; Y. Liu et al., 2013; Reichle et al., 2010; Slater & Clark, 2006). EnKF allows a dynamic update of state variables based on the model and the observation errors. At each time step, the model states (i.e., SWE) are updated based on the covariance of the errors between the modeled and the observed variables, then the model is run with the updated values to ensure internal consistencies in mass and energy closures. The one-dimensional formulation of EnKF consists of assimilating the variables at each grid cell independently while neglecting the spatial correlations (Reichle & Koster, 2003). We follow the assimilation of snow variables as described by Kumar et al. (2014, 2019). To represent the model uncertainties and the observation errors, a model ensemble of size 20 was created by perturbing the hourly meteorological forcing inputs (the ensemble precipitation, and the downscaled air temperature, and downward longwave and shortwave radiation), the modeled, and the observed hourly snow variables. Following Kumar et al. (2019), we use a multiplicative perturbation with a mean of 1 and a standard deviation of 0.5 for the precipitation field. A multiplicative perturbation is also used for the downward shortwave radiation, the mean is equal to 1 and the standard deviation 0.2. Air temperature and downward longwave radiation are perturbed using additive perturbation with a standard deviation equal to 0.5° and 30.0 W/m^2 respectively. The modeled SWE and snow depth are perturbed with a multiplicative noise of 0.01. A cross-correlation with a coefficient of 0.9 is set for the modeled SWE and snow depth. The observed SWE is perturbed with a multiplicative noise of 0.05. All simulations are performed using the NASA Land Information System (LIS; Kumar et al., 2006).

HMA is a data scarce region, where reliable ground measurements are rare and sparse, making model validation against observations difficult. A limited model evaluation is presented here using remote sensing datasets and reanalyzes. The modeled snow cover estimates are compared using the MODIS snow data version 6 (Hall et al., 2006). Specifically, we compute the percentage of snow cover detected correctly and incorrectly, using a detection threshold of 0.1 snow cover fraction. We assume that snow cover is correctly detected at a single model cell if both the model and MODIS have a snow cover fraction greater than 0.1. False snow detection is identified if the model indicates that the cell is snow-covered (i.e., the snow cover fraction is greater than 0.1) whereas MODIS indicates no snow cover. In addition, the signs of the trends in the water available for runoff were compared to the signs of the trends in the runoff provided by Ghiggi et al. (2021). Because of the differences in the definitions of "runoff" between our study (which is the water available for runoff) and Ghiggi et al. (2021), we only compared the sign of the trends, not their magnitudes. Note that extensive evaluations of the precipitation data used in this study have been presented in Maina, Kumar, Dollan, and Maggioni (2022), which demonstrates that the ensemble precipitation allows for a better representation of the ground measured precipitation, particularly in the yearly trends and averages.

2.2.2. Definition and Identification of ROS

There is no consensus on the definition of ROS in prior studies. Consequently, several methods have been reported in the literature for quantifying ROS. In addition, some studies focus on ROS event (Freudiger et al., 2014;

McCabe et al., 2007) whereas others use the term ROS day (Musselman et al., 2018). The quantifications of ROS events or days mainly require a minimum threshold for both rainfall and snowpack, whereas, the snowmelt resulting from a ROS is also used in some studies (Freudiger et al., 2014; McCabe et al., 2007; Musselman et al., 2018; Würzer et al., 2016). These thresholds depend on the characteristics of the studied region and its climate. Following Musselman et al. (2018), we define ROS day as a day where at least 10 mm of rain (i.e., total rainfall during the day) falls on an at least 10 mm snowpack. In Noah-MP, precipitation is partitioned into rainfall and snowfall using Jordan's scheme (Jordan, 1991). In this study, we quantify the monthly values (then their corresponding annual averages) of:

- ROS ratio is defined as the ratio of the total rainfall identified as ROS during the month and the total precipitation (P) of the month

$$\text{ROS ratio} = \frac{\text{ROS}}{P} \tag{1}$$

- ROS Snowmelt ratio is defined as the ratio of the total snowmelt occurring the day after a ROS day (i.e., ROS snowmelt) during the month and the total snowmelt of the month

$$\text{ROS Snowmelt ratio} = \frac{\text{ROS Snowmelt}}{\text{Snowmelt}} \tag{2}$$

- Snowmelt contribution to the water available for runoff is defined as the ratio of the total snowmelt of the month and the sum of total rainfall and snowmelt of the month following Mazurkiewicz et al. (2008) and Musselman et al. (2018)

$$\text{Snowmelt contribution to water available for runoff} = \frac{\sum\limits_{k=1,n\text{day}} \text{Snowmelt}}{\sum_{k=1,n\text{day}} \text{Rainfall} + \text{Snowmelt}} \tag{3}$$

where $n$day is the total days of the month

- ROS snowmelt contribution to the water available for runoff is defined as the ratio of the total snowmelt occurring the day after a ROS day (i.e., ROS snowmelt) during the month and the sum of total rainfall and snowmelt of the month

$$\text{ROS Snowmelt contribution to water available for runoff} = \frac{\sum_{k=1,n\text{day}} \text{ROS Snowmelt}}{\sum_{k=1,n\text{day}} \text{Rainfall} + \text{Snowmelt}} \tag{4}$$

2.2.3. Statistical Analyses: Computation of the Trends

To quantify the evolution of ROS in HMA over the past two decades, we computed the trends in ROS amounts and days using the Mann-Kendall test which determines whether a time series has a monotonic upward or downward trend (Kendall, 1948; Mann, 1945; Yue et al., 2002). The Mann-Kendall trend test is computing using the following formula:

$$S = \sum_{i=1}^{n-1} \sum_{j=k+1}^{n} \text{sign}(x_j - x_i) \tag{5}$$

where x is the time series variable. The subscript j and k are the observation time. $\text{sign}(x_j - x_i)$ is equal to $+1$, 0, or -1, which means increasing, no, and decreasing trends, respectively. In this study, we assumed that there is no significant trend in the data at 95% confidence level (or at a significant level of 5%). To better understand the trends in ROS, we also compute the trends in precipitation, snowfall, rainfall, ROS, temperature, seasonal snow cover, snow depth, snowmelt, and ROS snowmelt.

3. Results

3.1. Model Evaluation

Appendix A illustrates the comparisons between simulated and remotely sensed snow cover. We investigate the snow detection accuracy of our model (Figure A1). Our results indicate that the percentage of correctly detected

snow cover is generally high, varying between 60% and 80% (Figure A1a). The highest ratio is from May to September, which corresponds to the period where snow cover is high in majority of HMA's basins. Figures A1b and A1c depict the spatial distribution of the probabilities of detection and false alarm. Overall, the probability of detection is greater than 60% in most areas, and the probability of false alarm remains low (<40%). The high values in probability of detection and low values of probability of false alarm are further highlighted when these evaluations are stratified by different seasons (Figure A1d). During the periods when snow cover is considerable (DJF and MAM), the probability of detection over the mountain terrain is high (>80%) while the probability of false alarm is low (<30%). Note that areas with high rates (in terms of annual averages) of false alarm in snow cover (i.e., the model shows a snow-covered area while MODIS indicates no snow) are mainly located in mid to low elevations where the snow cover is low and ephemeral (Figure A1e). This is also illustrated in Figure A1f, where the probability of detection of snow cover is stratified by month and by elevation bands. During peak winter months and over high elevation areas, the snow detection accuracy is high. Areas with high false alarm probability are also found in the Tibetan plateau where the ratio of the seasonal snow cover remains low that is, less than 20% on average (Figures A1b–A1d).

Appendix B (Figure B1) illustrates the trends in runoff computed with the data provided by Ghiggi et al., 2021 and the results of our model (Noah-MP with assimilation). The sign of the trends in runoff over the Ganges-Brahmaputra basin are consistent with Ghiggi et al. (2021), The eastern part of the Ganges-Brahmaputra basin corresponding to the Brahmaputra basin is characterized by a decreasing trend whereas the western areas (i.e., the Ganges basin) have increasing trends. Also, the increasing trends in the simulated runoff over the Indus, the Yangtze, and the Hwang Ho basins agree with Ghiggi et al. (2021). However, while the northwestern basins are characterized by positive and statistically no significant trends in results of Ghiggi et al. (2021), our results indicate positive and negative trends. These differences between our study and that of Ghiggi et al. (2021) in the northwestern basins could be related to the impacts of irrigation occurring in these basins and water infrastructures (Jalilov et al., 2016; White et al., 2014).

The assimilation of SWE has also been shown to improve the representation of both snow variables and runoff (Figures C1–C3).

3.2. Spatial Patterns of ROS in HMA and Its Seasonality

Because of its complex orography, HMA has a complex precipitation pattern controlled by both westerlies and monsoons. The spatial distributions of precipitation are highly heterogeneous in the region with high precipitation mostly located in the Irrawaddy basin and the eastern Ganges-Brahmaputra (Figure 2a). The Himalayas are also characterized by high precipitation. Most of the precipitation falls as snow in the Tibetan plateau and its surrounding mountains, the Himalayas and Tien Shan corresponding to the areas where the elevation is above 4,000 m. Precipitation days in HMA exceed 300 days/year, especially in the east and the Tibetan Plateau (Figure 2a). ROS only occurs in the Himalayas, Karakoram, Pamir, and Tien Shan covering the Ganges-Brahmaputra, Indus, Amu Darya, Syr Darya, and Ili basins. On average, over the studied period, 10% of total amount of precipitation is ROS. ROS occurs around 30 days per year and mostly in the northwestern basins. Only a small fraction of the Ganges-Brahmaputra is subject to ROS.

To study the monthly variations of ROS in HMA, we illustrate in Figure 2b the average (over the studied period) monthly variations of the ratio of the amount of ROS and precipitation in 5 basins where ROS occurs. Figure 2b also illustrates the ROS snowmelt ratio defined in Section 2.2.2.

In the Indus basin, precipitation has two peaks, in April and in September (Appendix D, Figure D1). Most of the precipitation falling in April is snowfall; rainfall starts in February with a peak in August. Nonetheless, snowfall represents approximately 50% of the precipitation on average in the basin. ROS in the Indus is less than in the other basins. Throughout the year, less than 5% of the total amount of precipitation is ROS over the Indus on average, with the highest occurrence from June to August where more than 30% of the total precipitation is ROS. Snowmelt in the Indus occurs from February to September. The ROS snowmelt is non-negligible and its ratio reaches up to 30% in February and March. This ratio decreases as fewer ROS days happen from March to June. In July with the increase in both ROS days and amounts, the ROS snowmelt ratio exceeds 20%. Although most of the ROS occur from June to August in the Indus basin, ROS days from January to March have the highest contribution to the snowmelt because of the shallow depth of the snowpack and the low temperatures; As a result,

10.1029/2022EF003009

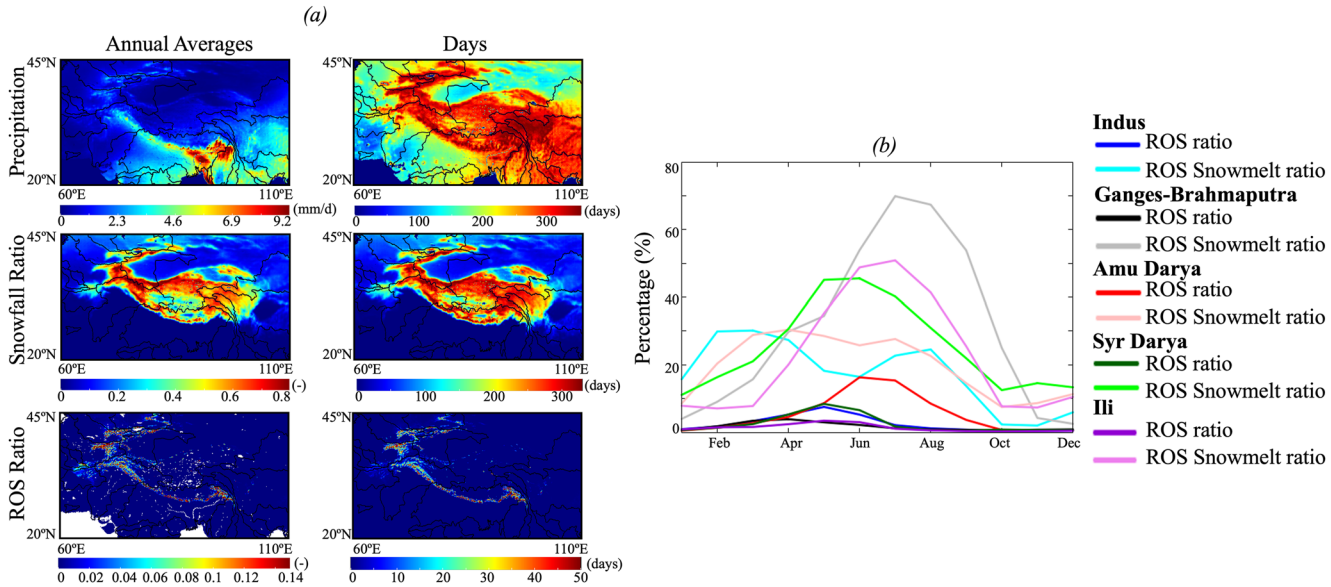

Figure 2. (a) Spatial distributions of annual average (i.e., mean of the 18 years) and total of number of days of precipitation (i.e., days with a nonzero precipitation), the ratio of the amount of snowfall over the amount of precipitation, and the ratio of the amount of rain-on-snow (ROS) over the amount of precipitation. Note that we showed the total number of days of snowfall and ROS. (b) Monthly variations of the ratio of the amount of ROS over the amount of precipitation (ROS/P) in percent and the ratio of the amount of snowmelt after ROS over the total monthly snowmelt (ROS/Snowmelt) in percent in basins where ROS events occur in High Mountain Asia.

the snowmelt is only triggered by ROS. Nonetheless, ROS has also a noteworthy contribution to the snowmelt in summer because it happens after the snow has started to melt, and hence, ROS accelerates the melting.

Contrary to the Indus, the Ganges-Brahmaputra basin has one peak of precipitation occurring in July, a period during which the precipitation mostly falls as rain (Appendix D, Figure D1). Winter precipitation is mostly snowfall. ROS represents on average 11% of the total annual precipitation and mainly occurs from April to September with the highest ROS occurrence and amount in August a period during which ROS represents more than 40% of precipitation. Snow melts year-round in the basin, but the highest snowmelt is in July. Throughout the year, the ROS snowmelt ratio exceeds 10%, and in summer it is greater than 60%. Therefore, ROS considerably (>50%) contributes to the snowmelt in this region because of the timing of its occurrence as in the Indus basin.

ROS represents less than 10% of the annual precipitation on average of the northwestern basins (i.e., Amu Darya, Syr Darya, and Ili). In these basins, because the winter precipitation is higher than in the Indus and the Ganges-Brahmaputra, ROS mainly occurs in late winter and spring (from February to June). In the Amu Darya, ROS lasts until September but with low frequency and amount. At the peak of ROS in June, it represents around 38% of precipitation. As precipitation stops early compared to the basins previously studied (i.e., summer precipitation is low compared to the Indus and the Ganges-Brahmaputra), the peak of snowmelt occurs in June. The contributions of ROS to snowmelt are high in May (the ROS snowmelt ratio is higher than 30% in the Amu Darya and 40% in the Syr Darya and Ili).

The five basins subject to ROS in HMA have different dynamics. ROS is more frequent and higher in the northwest. In Amu Darya, Syr Darya, and Ili basins, ROS mainly occurs in late winter and spring, a period during which it contributes up to 40% to the snowmelt. In the Ganges-Brahmaputra, ROS considerably contributes (up to 60%) to the snowmelt. This is because ROS mainly occurs in summer when the snowpack has already started to melt, therefore ROS exacerbates this melt. ROS in the Ganges-Brahmaputra has similar temporal patterns as in the Indus where it represents 5% of precipitation and contributes to more than 20% of snowmelt.

3.3. Yearly Trends in ROS Ratio and ROS Snowmelt Ratio Over the Past Decades in HMA

Figure 3 depicts the statistically significant trends in precipitation, the ratio of snowfall and precipitation, temperature, seasonal snow cover, the ratio of the total amount of ROS and precipitation, and the ROS snowmelt ratio. Precipitation trends in HMA are bidirectional; the eastern region and the Indus see an increase (up to

10.1029/2022EF003009

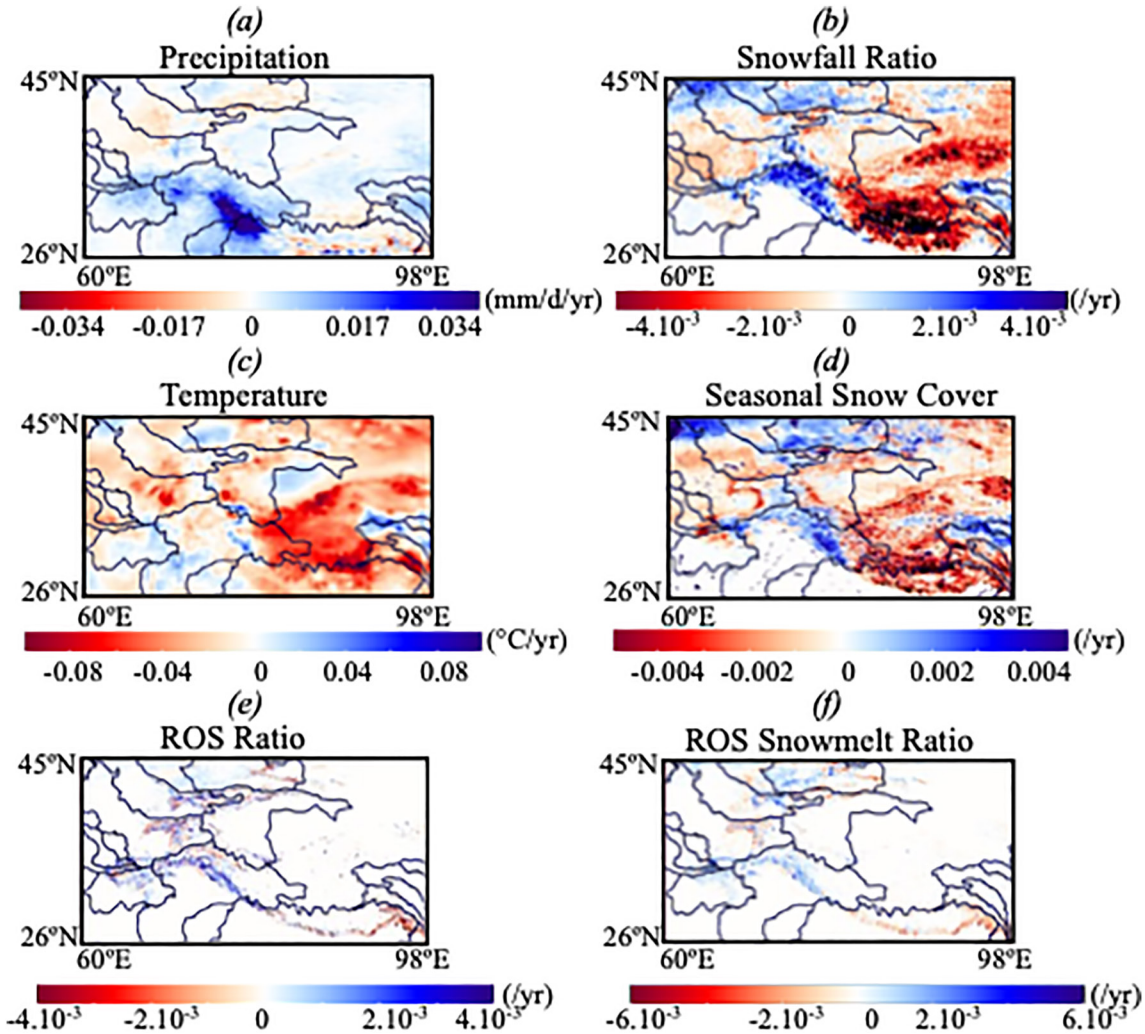

Figure 3. Spatial distributions of the yearly trends in (a) precipitation, (b) the ratio of snowfall over precipitation (Snowfall/Precipitation), (c) temperature, (d) seasonal snow cover, (e) the ratio of rain-on-snow (ROS) over precipitation (ROS/Precipitation), and (f) the ratio of snowmelt after ROS over the total monthly snowmelt in basins where ROS events occur (ROS/Snowmelt). Trends were computed using the Mann-Kendall test with a confidence level of 95%, non-significant trends were set to 0.

0.04 mm/d/yr), whereas the Ganges-Brahmaputra and the northwest have decreasing (up to 0.02 mm/d/yr in the Ganges and less then 0.01 mm/d/yr on average in the northwest) trends in precipitation (Figure 3a). As shown in Figure 3c, the temperature increases almost everywhere in HMA at a rate higher than 0.02°C/year. Snowfall also decreases in the Ganges-Brahmaputra (the snowfall ratio decreases by 0.002/yr on average) and in dispersed areas of the northwestern basins due to both decreases in precipitation and increases in temperature. In the Indus basin, the temperature has a slight increase at a rate lower than 0.01°C/year. This increase in temperature is, however, not sufficient enough to trigger a change in the precipitation phase. As a result, the increase in precipitation over the Indus results in an increase in snowfall equal to 0.0025 on average. The trends in the seasonal snow cover matches the trends in snowfall previously discussed. The trends in the ratio of ROS and precipitation are similar to the trends in the ratio of snowfall and precipitation. Both ROS amounts and days (note the trends in ROS days have not been shown here due to their similarity to the trends in the ratio of ROS and precipitation) have decreasing trends in the Ganges-Brahmaputra (0.001/yr on average) and increasing trends (>0.002/yr) in the Indus basins. ROS trends in the northwestern basins are bidirectional, with ROS decreasing (inferior to 0.001/yr) in low elevation areas, and an increasing trend in high elevation areas (up to 0.0025/yr) close to the water towers. This is because snowpack decreases in low elevations areas as a result of warming and a decrease in precipitation (as illustrated in Figure 3a). As the snowpack is persistent despite the increasing trends in temperature in high elevation zones, hence the increase in precipitation and shift in precipitation phase (i.e., more precipitation is falling

10.1029/2022EF003009

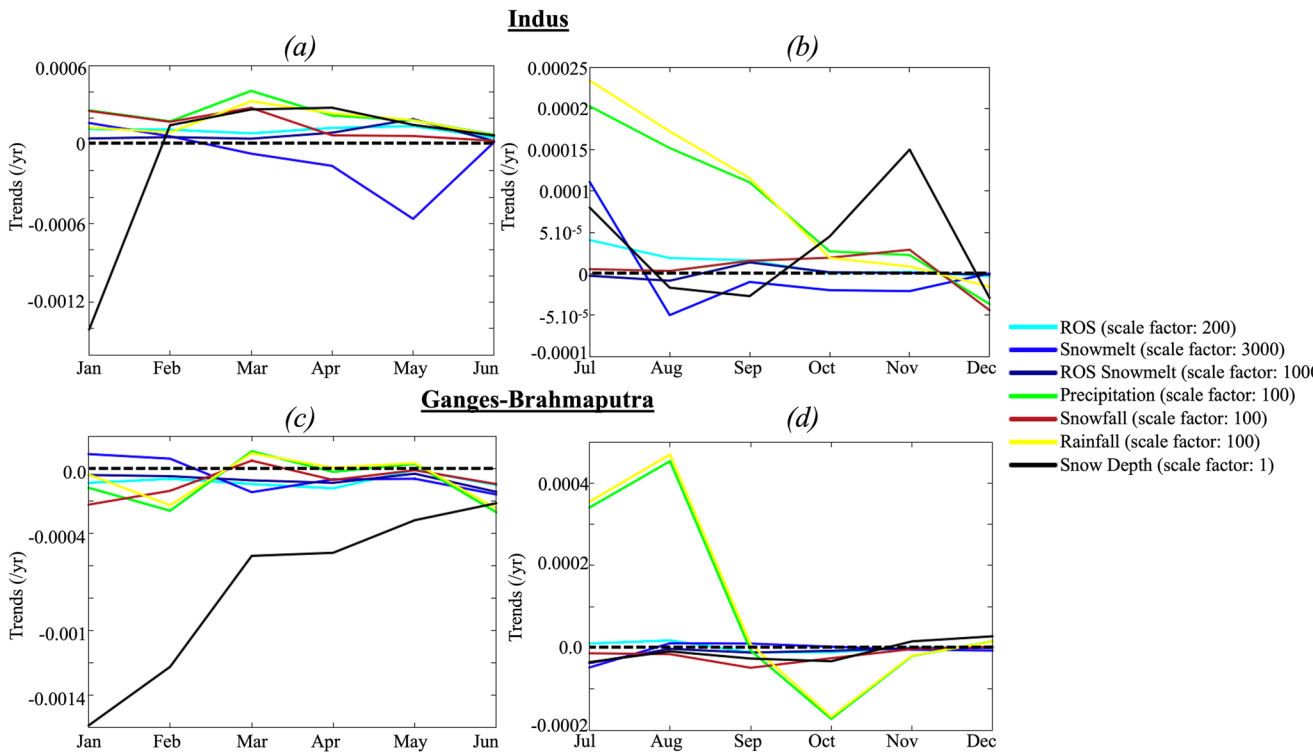

Figure 4. Monthly variations of the trends in rain-on-snow (ROS), snowmelt, snowmelt after ROS events, precipitation, snowfall, rainfall, and snow depth in the Indus (a) from January to June and (b) from July to December and in the Ganges-Brahmaputra (c) from January to June and (d) from July to December. Trends were computed using the Mann-Kendall test with a confidence level of 95%, cells with non-significant trends were set to 0 in the calculation of the basin average. Note that the actual values of trends have been rescaled to match the min and max values of the *y* axis.

in the form of rainfall) leads to more ROS amount. In addition to following the elevation patterns, the trends in ROS are also related to the trends in rainfall, with ROS increasing in areas characterized by increased rainfall. Trends in ROS snowmelt ratio follow the trends in ROS, with more snowmelt related to ROS in the Indus (the ROS snowmelt ratio increases by 0.0015/yr) and less in the Ganges-Brahmaputra (with a decreasing trend equal to 0.0021/yr on average). Similarly, in the northwest, the trends in snowmelt caused by ROS are bidirectional with dispersed negative (>0.0015/yr) and positive (~0.002/yr) values as the trends in ROS.

3.4. Monthly Trends in ROS and ROS Snowmelt Over the Past Decades in HMA

To further examine the changes in ROS in HMA, the monthly trends in precipitation, rainfall, snowfall, snow depth, ROS, snowmelt, and ROS snowmelt in the Indus and Ganges-Brahmaputra are shown in Figure 4 (with the other basins shown in Appendix E, Figures E1a–E1f). Due to the differences in the scales and values of trends between the winter and the summer, we split the monthly variations in two from January to June and from July to December. In the Indus, though precipitation is generally increasing everywhere as mentioned previously, a slight decrease equal to 0.04 mm/d/yr is noted in December. This increase in precipitation (reaching 0.2 mm/d/yr in July) triggers both increases in rainfall (~0.21 mm/d/yr) and snowfall (~0.18 mm/d/yr). Nonetheless, the increase in rainfall is higher than the increase in snowfall. Snow depth increases (<0.01 cm/yr) from February to July, then shows a decreasing trend (equal to 0.0025 cm/yr on average) in August and September. Moreover, snow depth tends to decrease in January and December. Despite the bidirectional trend in snow depth throughout the year, ROS is increasing every month (at a rate up to 0.03 mm/d/yr) due to the persistence of snow on the ground. Although snow depth decreases, there is still a remaining snowpack, which with more precipitation falling as rainfall, led to ROS. The decreasing trend in snow depth in August and September occurs despite increasing snowfall due to the occurrence of ROS. The latter enhances the snowmelt as shown by its increasing trends, especially in September. As ROS stops in September, increasing snowfall leads to an increase in snow depth. The consequences of the increasing trends in ROS stemming from an increasing rainfall are therefore a decrease in

10.1029/2022EF003009

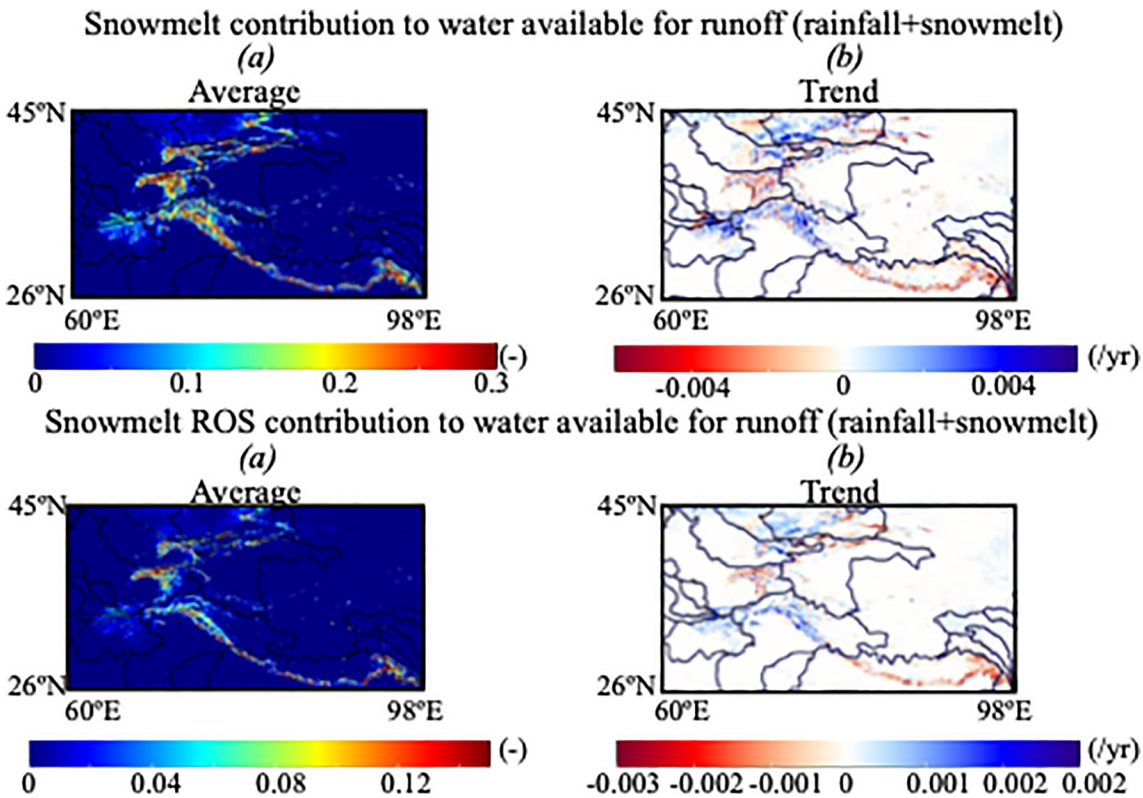

Figure 5. Spatial distributions of the (a, c) averages (i.e., mean of the 18 years) and (b, d) trends in the contributions of snowmelt and respectively the snowmelt occurring the day after a rain-on-snow day to the water available for runoff defined as the sum of the total rainfall and snowmelt. Trends were computed using the Mann-Kendall test with a confidence level of 95%, non-significant trends were set to 0.

the snowpack in summer. This could potentially shorten the snowpack duration and lead to early snowmelt with considerable consequences for the water available for runoff.

In the Ganges-Brahmaputra, the precipitation is decreasing (0.15 mm/d/yr) in almost all the months except in July and August (0.39 mm/d/yr), when the rainfall increases. The consequence of the decreasing trends in precipitation and snow depth (up to 0.15 cm/yr) is a decreasing trend in ROS (up to 0.12 mm/d/yr in April). Because the snowpack is shrinking, the decreasing rainfall does not fall on snow.

3.5. Implications for the Water Available for Runoff

In this section, we discuss the implications of ROS for the water available for runoff in HMA. Figure 5 illustrates (a) the annual average of the snowmelt's contribution to the water available for runoff (see definition in Section 2.2.2) and (b) the corresponding statistically significant trends and (a) the annual average of the ROS snowmelt contribution to the water available for runoff (see definition in Section 2.2.2) and (b) the corresponding statistically significant trends. Snowmelt significantly contributes to the water available for runoff in the HMA. In the Indus basin, around 10% of the total water available for runoff originates from snowmelt whereas this percent reaches 30% in the Ganges-Brahmaputra. Similarly, the snowmelt represents more than 30% of the total water available for runoff in the northwestern basins. The spatial distributions of the average of the snowmelt's contribution to the water available for runoff and the ROS snowmelt contribution to the water available for runoff are similar. As discussed in Section 3.2, the Ganges-Brahmaputra has the highest contribution of ROS snowmelt to the water available for runoff with more than 10% in many areas. In the Indus basin, the contribution of the ROS snowmelt to the total water available for runoff is less than 10% in many areas. The trends in the contributions of the total snowmelt and the total ROS snowmelt are akin and similar to the trends in ROS amounts and snowfall previously discussed. As such, the Ganges-Brahmaputra basin and the Indus basin have two distinct and opposite trends. Because both snowfall and ROS decrease in the Ganges-Brahmaputra the contributions of

snowmelt decreases (>0.004/yr.), that is, the contribution of rainfall to the water available for runoff increases more than that of snowmelt, contrary to the Indus basin where ROS increases the contribution of snowmelt to the water available for runoff (>0.002/yr). The trends in these contributions are bidirectional in the northwestern basin following the trends in ROS.

These results strengthen the conclusions drawn previously. Although ROS enhances snowmelt which has a noteworthy contribution to the total water available for runoff in the Ganges-Brahmaputra, these contributions decrease contrary to the Indus basin characterized by a low contribution of snowmelt to the total water available for runoff. Changes in ROS could shift the timing of runoff, however, in this study, we did not observe any considerable shift in the timing of hydrologic processes. This probably stems from the relatively short period of time we have investigated ∼18 years.

4. Discussion

4.1. Comparisons With Previous Studies and Model Uncertainties

The trends observed in this work agree with previous studies. First, the bidirectional trends in precipitation are consistent with Nguyen et al. (2018). Second, snowfall increases in the Indus basin have been documented in previous studies which employ datasets and models different from the ones used in this study (Maina, Kumar, Albergel, & Mahanama, 2022; Smith & Bookhagen, 2018). Also, the trends in seasonal snow cover are consistent with increasing trends in snow cover remotely sensed by MODIS (Hall et al., 2006; Kraaijenbrink et al., 2021; Maina, Kumar, Albergel, & Mahanama, 2022) and the trends in the water available for runoff are in agreement with the global runoff data developed by Ghiggi et al. (2021). Finally, the patterns of ROS in HMA we observed, such as the relationship between elevation and the trends in ROS, are in agreement with previous studies focusing on North America (Musselman et al., 2018; Surfleet & Tullos, 2013).

Despite the consistency with prior results, we acknowledge that our model estimates also likely have irreducible uncertainties. The lack and/or the limited amount of available and reliable remote sensing products and ground measurements of hydrologic variables make the model evaluation and comparison difficult to perform in this region. The complex orographic patterns of HMA affect the performance of reanalyzes and remotely sensed variables and induce high biases. As a result, our model evaluation was limited to MODIS snow cover product. Though this evaluation is not comprehensive, it allows to assess the performance of our model in reproducing a critical variable associated with ROS, that is, snow. Note that the SWE reconstruction we have used in this study has been evaluated in previous studies (Kraaijenbrink et al., 2021). Another source of uncertainty in our results is the meteorological forcing that we used. Due to the complexities of the atmospheric and land surface processes in HMA, accurate estimation of precipitation and other meteorological forcing is difficult and different forcings lead to different results. This issue has also been widely discussed in the literature (Maina, Kumar, Dollan, & Maggioni, 2022; Yoon et al., 2019; You et al., 2015). The uncertainties from the forcing meteorology are reduced by using an ensemble generated with reasonable gridded precipitation datasets, described in detail in Maina, Kumar, Dollan, and Maggioni (2022). Because our study relied on remote sensing products that are only available for a short period of time (i.e., less than 20 years), we could not investigate the longer-term trends in ROS and their impacts on hydrology. As a result, some potential impacts of ROS such as the shift in the timing of surface runoff and/or seasonality of hydrologic states and fluxes were not quantified.

Dust and other dark particles such as black carbon have been shown to play an important role in the snow dynamics in HMA by darkening the snowpack and subsequently accelerating the snowmelt (Sarangi et al., 2020). These non-climate-related dynamics are difficult to model because of the lack of data notably the spatiotemporal changes of dust and black carbon. Although dust and black carbon could contribute to the decrease in snowpack in the Himalayas, particularly in the Indus basin as shown in previous studies (Sarangi et al., 2020), the observed decreasing trends in snowpack in summer in the Indus basin despite an increase in snowfall is due to ROS that accelerates the melting of the snow and hence it decreases.

4.2. Implications for Downstream Hydrology

ROS in HMA is more frequent (up to 50 days of ROS per year) than in the western US (less than 15 days, Musselman et al., 2018) yet ROS and its consequences are most of the time overlooked in the region. ROS

considerably contributes to snowmelt, especially in the Ganges-Brahmaputra where the ROS snowmelt ratio is higher than 60%. With the shift in the precipitation phase (with more precipitation falling as rain), careful consideration should be given to ROS and its impacts over HMA. Because of its persistent snowpack and increases in precipitation, ROS is increasing in the Indus basin. ROS mainly occurs in summer and its occurrence decreases the snowpack and enhances the snowmelt. Because the increases in ROS in the Indus shorten the duration of the snowpack and increases snowmelt, it, therefore, has the potential to decrease the soil moisture in the basin as the snowpack decreases earlier. Though we do not observe this impact on soil moisture now, this could arise in the future as the snowpack shrinks and the temperature warms. ROS could decrease soil moisture and induce drought in the Indus basin subject to intense agricultural activities with high rates of applied irrigated water (Salmon et al., 2015). This could lead to more irrigation demand which can have dramatic consequences on the already pronounced groundwater depletion (Rodell et al., 2009) and changes in land surface structures such as greening and changes in surface radiation (Maina, Kumar, Albergel, & Mahanama, 2022). We further note that in many areas where ROS occurs, the ROS snowmelt ratio represents more than 5% of the total water available for runoff defined as the sum of rainfall and snowmelt and can reach up to 15%. As a result, ROS considerably contributes to the water available for runoff in the region and its increasing trends should be accounted for in water management strategies. ROS-related floods will likely become frequent and previous studies have demonstrated the costly consequences of these floods in other regions (McCabe et al., 2007; Musselman et al., 2018; Sui & Koehler, 2001). Moreover, the increasing trends in ROS in the Indus basin have strong implications for landslides as the region is prone to these natural disasters (Kirschbaum et al., 2020; J. Liu et al., 2021). Landslides in HMA are usually caused by extreme precipitation and/or glacier melt in addition to earthquakes, freeze and thaw cycles, etc. With an increasing contribution of ROS to the total snowmelt, the impacts of ROS on landslides should be accounted for in landslides assessment studies. The contribution of ROS to the total water available for runoff is even higher in the Ganges-Brahmaputra compared to the Indus with more than 15% in many areas. On contrary to the Indus basin, ROS is decreasing in the Ganges-Brahmaputra due to the decreasing trends in snowpack and precipitation. However, ROS currently has serious implications for downstream hydrology as it considerably contributes to snowmelt and the water available for runoff in the basin. These high contributions of ROS to the total snowmelt and the water available for runoff may already be the causes of natural disasters such as floods and landslides in the basin, therefore, more studies analyzing the relations of these events to ROS are needed in the region. Like the Indus basin, the Ganges-Brahmaputra basin is also subject to agricultural activities and intense irrigation, the decreasing trends in ROS inducing decreasing trends in snowmelt will lead to a decrease in water availability. Unless the increasing trend in precipitation is sufficient enough to compensate for the decreases in snowmelt contributions, the decreases in recharge from the headwaters will increase the use of groundwater in the region, and exacerbate the observed dramatic consequences of an overuse of groundwater (Maina, Kumar, Albergel, & Mahanama, 2022; Rodell et al., 2009). Because of their bidirectional trends in ROS, both the Indus (characterized by increasing trends) and the Ganges-Brahmaputra (characterized by decreasing trends) ROS consequences could be locally observed in the northwestern basins.

5. Summary and Conclusions

The change in the precipitation phase due to global warming causes ROS in snow-dominated and mountainous regions such as HMA. ROS in HMA occur in five basins (Amu Darya, Syr Darya, Ili, Indus, and the Ganges-Brahmaputra). Because of the complexities of HMA, ROS dynamics are region-dependent:

- The Indus: in this basin where most of the precipitation falls as snowfall, ROS represents locally more than 5% of the annual precipitation and contributes up to 20% to the total annual snowmelt. ROS locally reaches up to 30% of precipitation in summer. ROS and its contributions to snowmelt are increasing in the region due to an increase in precipitation and a slight increase in temperature that is not enough to shift the precipitation phase. The increasing ROS in the Indus decreases the summer snowpack despite an increasing snowfall; therefore, ROS changes the snow dynamics of the region. Although ROS triggers early and high snowmelt in the Indus, it currently has little impact on the soil moisture of the region as it is subject to the monsoon that supplies more water in summer.
- The Ganges-Brahmaputra: in this basin where the snowfall represents around 30% of the precipitation, 11% of the annual precipitation is ROS. ROS mostly occurs in summer, and it considerably contributes to snowmelt up to 60%. ROS is decreasing in the Ganges-Brahmaputra because of the decreasing trends in precipitation and a declining snowpack.

- The northwestern basins (Amu Darya, Syr Darya, and Ili): ROS constitutes 5%–10% of the annual precipitation and mainly occurs in late winter and spring on contrary to the Indus and the Ganges-Brahmaputra where it occurs in summer. ROS locally contributes to up to 5% of the annual snowmelt with a high contribution in spring when more than 40% of the snowmelt is after a ROS. ROS and its contributions to snowmelt have bidirectional trends which depend on both trends in precipitation and elevation patterns.

This work sheds light on the dynamics of ROS in HMA, its trends, and its impacts on the snowpack and subsequently snowmelt. Future studies could investigate the impacts of ROS on floods and landslides as the region is prone to these natural disasters. Future studies could also evaluate the impacts of ROS on the vegetation dynamics in the region as the decreases in snowpack resulting from ROS could increase the growing season and leads to increasing soil moisture that will favor vegetation growth.

Appendix A: Comparisons Between Simulated and Remotely Sensed Snow Cover

We compare the simulated snow cover to the snow cover remotely sensed by MODIS. Figure A1 illustrates the high probability of detection and the low false alarm ratio of our model.

10.1029/2022EF003009

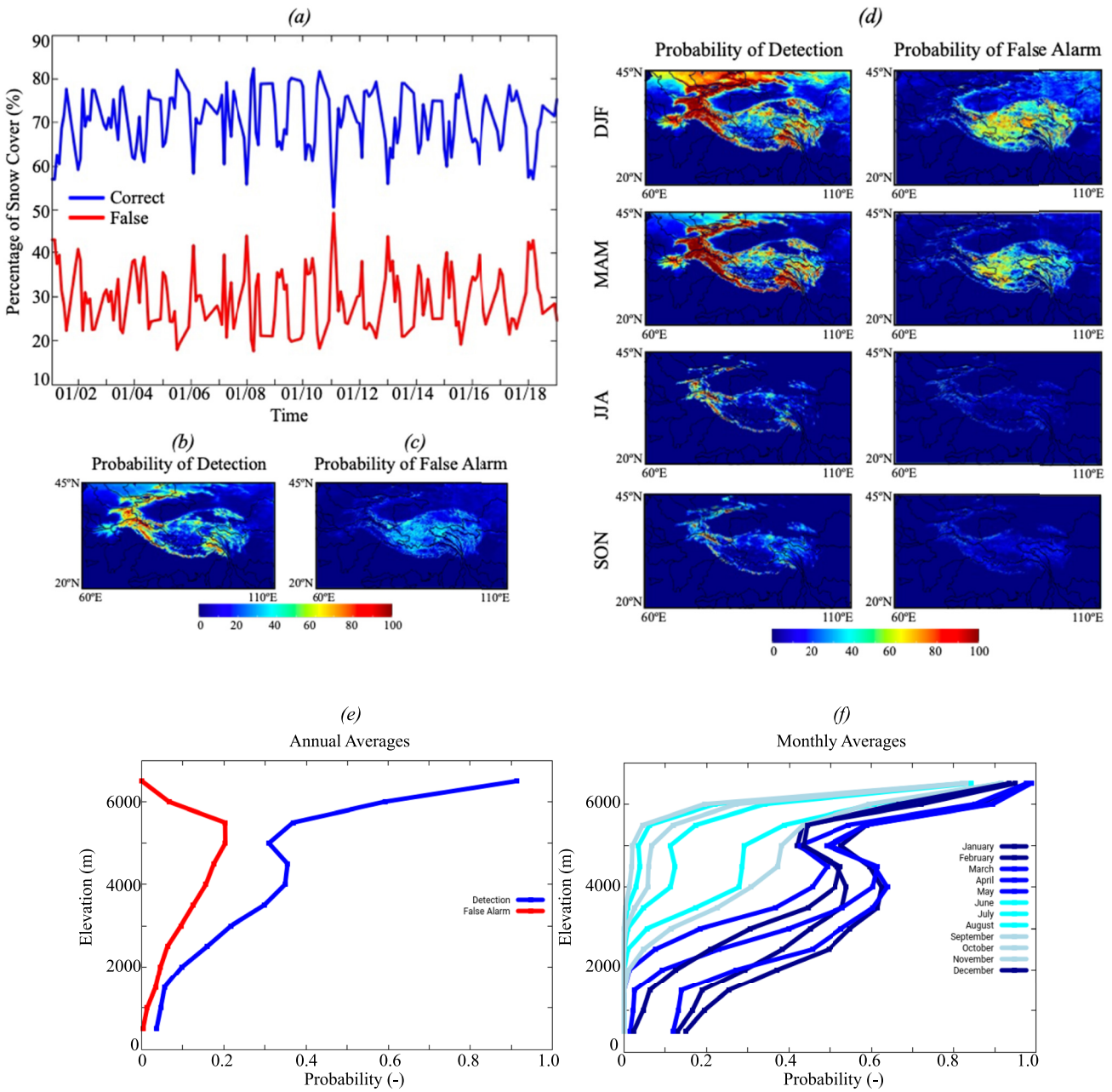

Figure A1. (a) Monthly variation of snow detection accuracy of the assimilation results compared to the snow cover provided by Moderate Resolution Imaging Spectroradiometer, and the spatial distribution of the probabilities of (b) detection (annual average), (c) false alarm (annual average), (d) the seasonal probabilities of detection and false alarm, (e) annual averages values of the probability of detection by elevation, and (f) the monthly values of the probability of detection by elevation.

Appendix B: Runoff Evaluation

The simulated runoff was evaluated by comparing it to the global runoff data provided by Ghiggi et al. (2021). Figure B1 shows that in general the trends in runoff of our model agree with the trends in the runoff by Ghiggi et al. (2021).

10.1029/2022EF003009

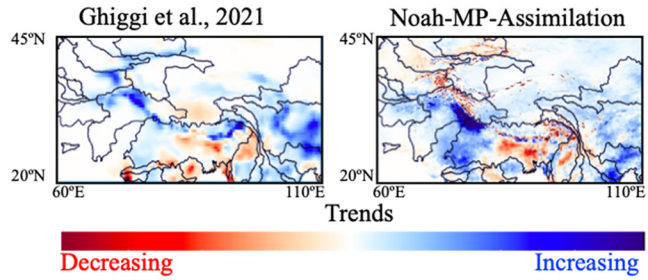

Figure B1. Comparisons of the signs of the trends in runoff provided by Ghiggi et al., 2021, and our model.

Appendix C: Comparisons Between the Assimilation and the Open Loop

The results of the assimilation of SWE were compared to an open loop simulation (i.e., simulation without assimilation). The assimilation of SWE improves the probability of the detection of snow and the trends in the runoff (Figures C1–C3).

10.1029/2022EF003009

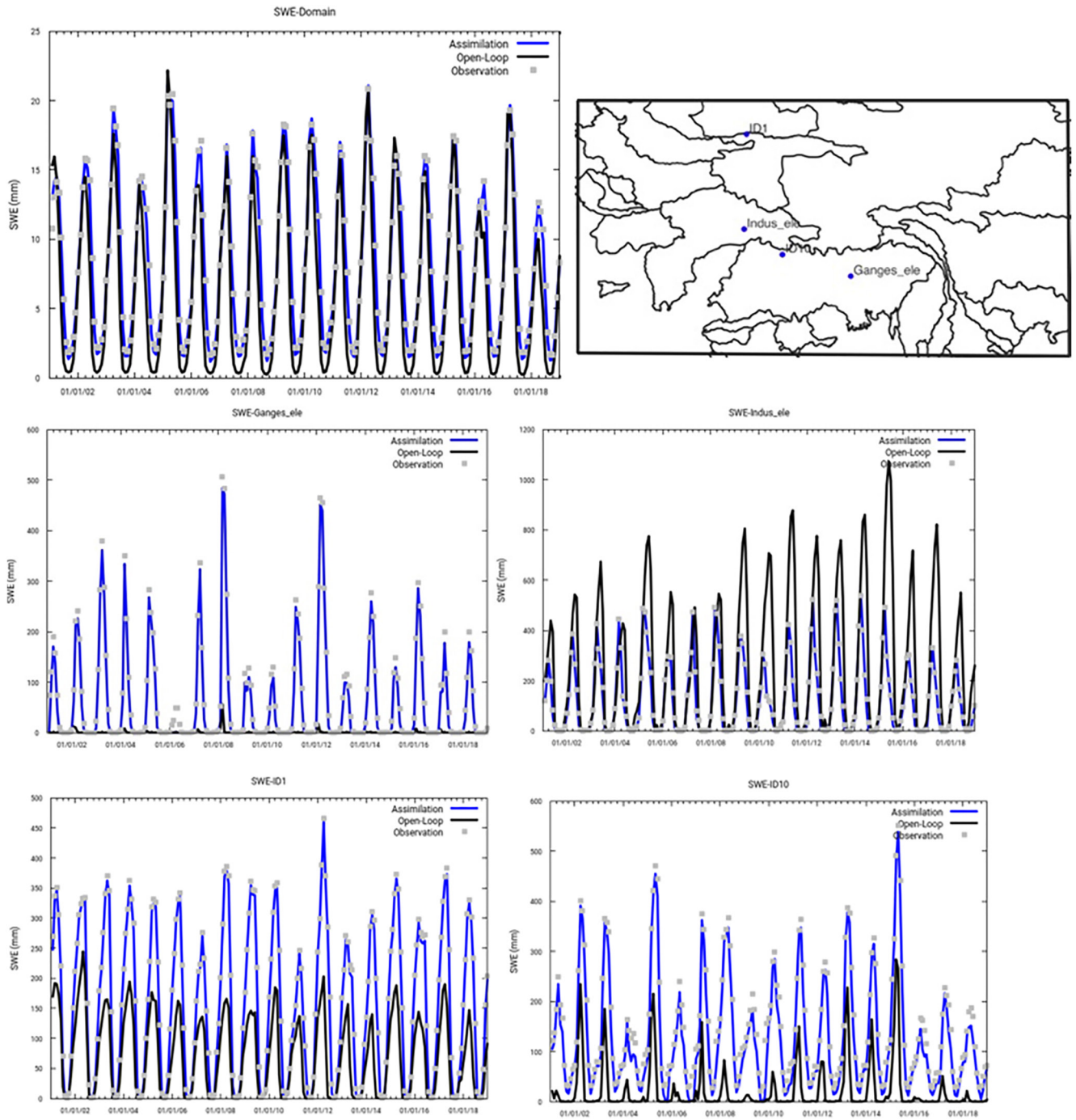

Figure C1. Comparisons of monthly values of snow water equivalent obtained with the open loop simulation, the assimilation and the observations (Kraaijenbrink et al., 2021).

10.1029/2022EF003009

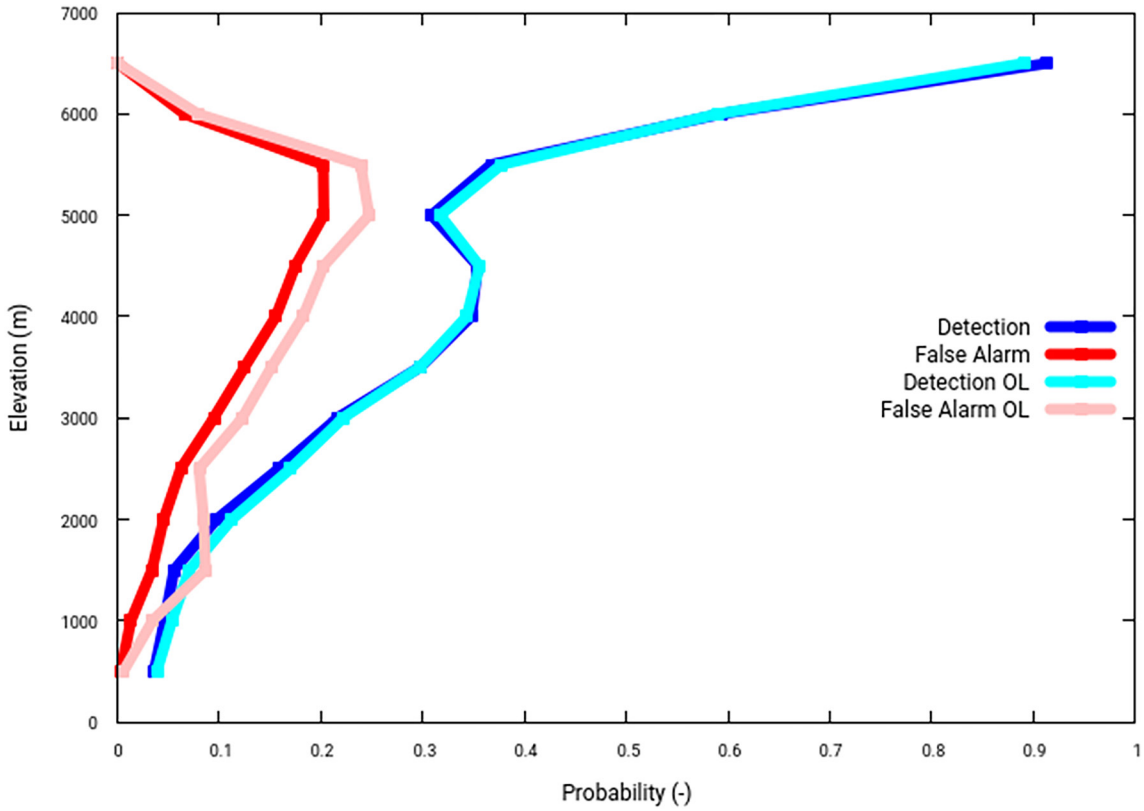

Figure C2. Comparisons of the probabilities of false alarm and detection associated the assimilation and the open loop.

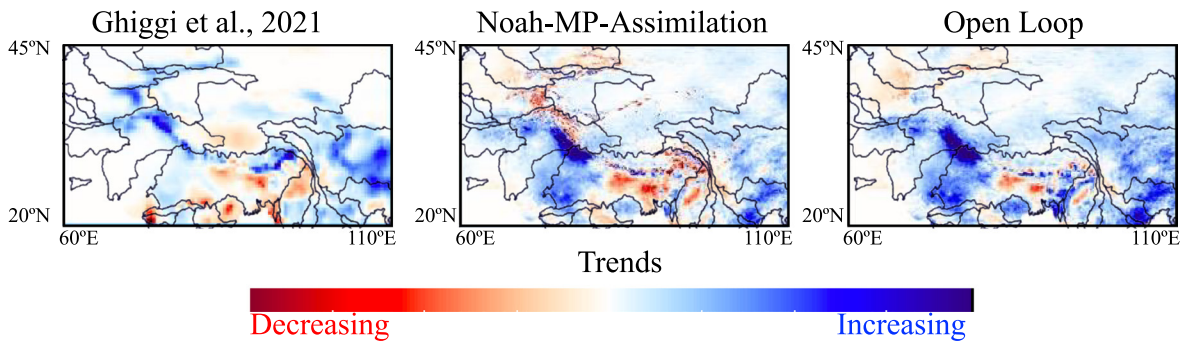

Figure C3. Comparisons of the signs of the trends in runoff computed by Ghiggi et al., 2021, the assimilation, and the open loop.

Appendix D: Monthly Variations of Precipitation, Snowfall, Rain-On-Snow (ROS), Snowmelt, Snowmelt After ROS

Figure D1 depicts the monthly variations of precipitation, snowfall, rain-on-snow, snowmelt, and snowmelt after rain-on-snow in the 5 HMA basins subject to rain-on-snow (Indus, Ganges-Bahmaputra, Amu Darya, Syr Darya, and Ili).

10.1029/2022EF003009

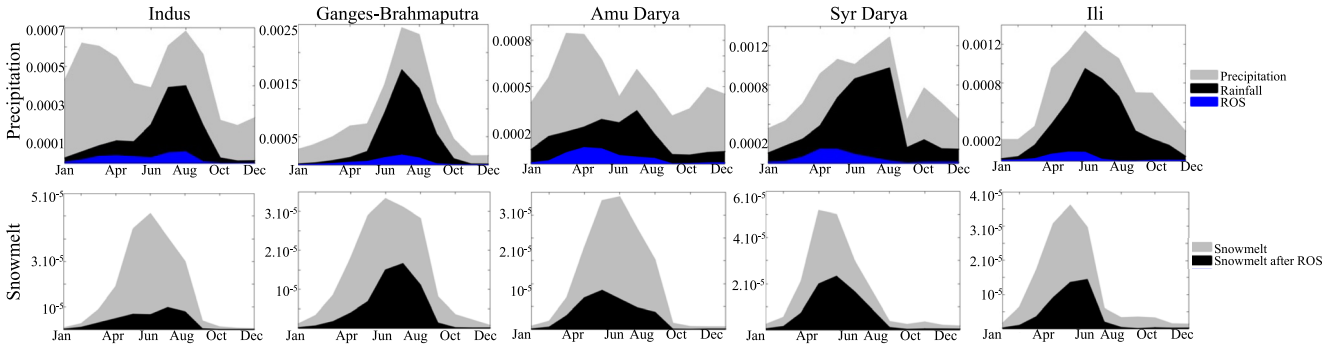

Figure D1. Monthly variations of the mean of precipitation, snowfall, rain-on-snow (ROS), snowmelt, and snowmelt after ROS.

Appendix E: Monthly Variations of the Trends in Amy Darya, Syr Darya, and Ili

Figure E1 illustrates the monthly variations of the trends in rain-on-snow, snowmelt, snowmelt after rain-on-snow, precipitation, snowfall, rainfall, and snow depth in Amu Darya, Syr Darya, and Ili.

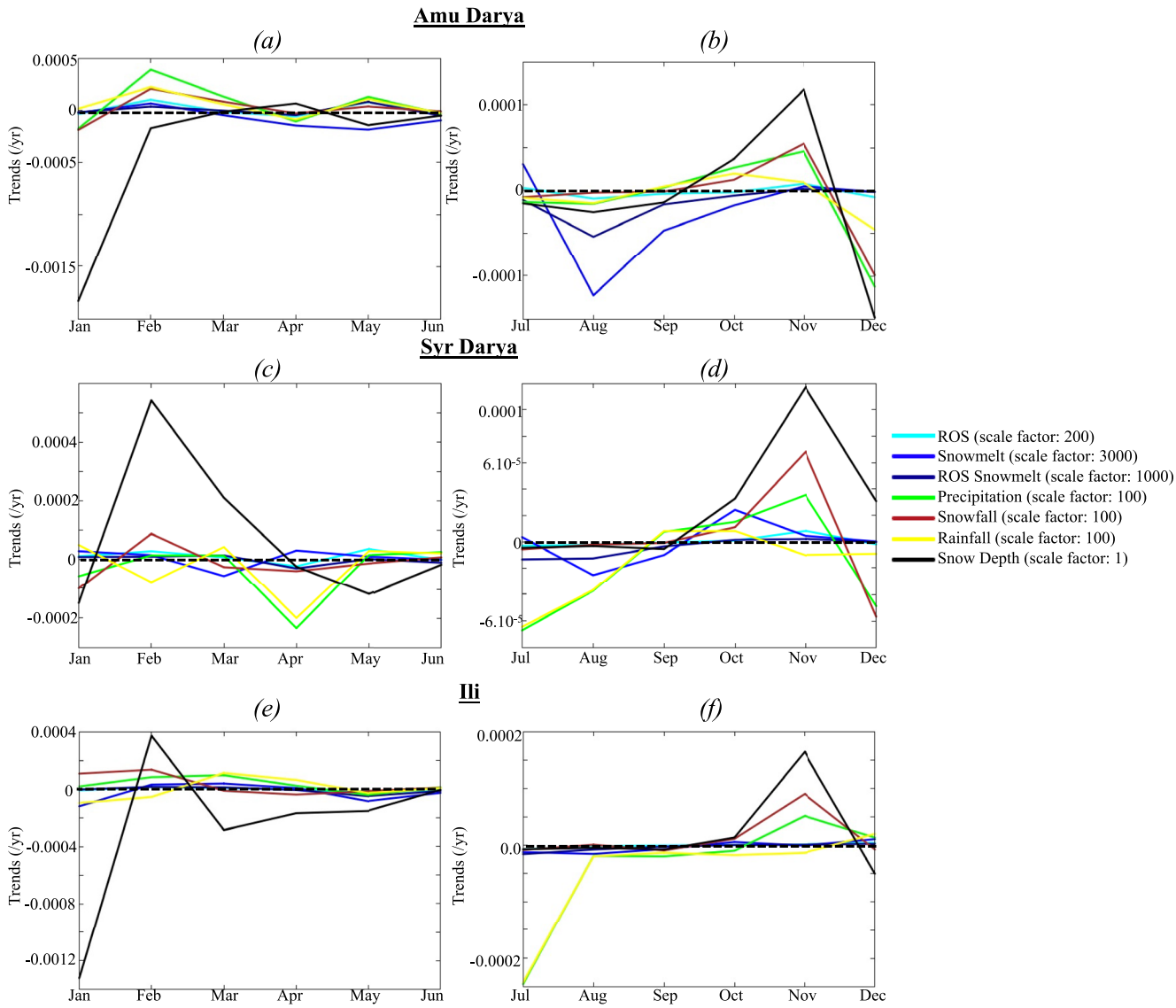

Figure E1. Monthly variations of the trends in rain-on-snow (ROS), snowmelt, snowmelt after ROS events, precipitation, snowfall, rainfall, and snow depth in the Amu Darya, Syr Darya, and Ili. Trends were computed using the Mann-Kendall test with a confidence level of 95%, cells with non-significant trends were set to 0 in the calculation of the basin average. Note that the actual values of trends have been rescaled to match the min and max values of the *y* axis.

Data Availability Statement

The Nasa Land Information System (LIS) used in this study is an open-source software that can be found here: https://github.com/NASA-LIS/LISF.

Datasets used in this study can be found in the following websites:

- ERA5 forcing: https://www.ecmwf.int/en/forecasts/datasets/reanalysis-datasets/era5
- IMERG Precipitation: https://gpm.nasa.gov/taxonomy/term/1372
- CHIRPS Precipitation: https://data.chc.ucsb.edu/products/CHIRPS-2.0/global_daily/netcdf/p05/
- SWE reconstruction by Kraaijenbrink et al. (2021): https://zenodo.org/record/4715786#.YqDY0S-B1pI

Acknowledgments
This research was supported by funding support from the National Aeronautics and Space Administration High Mountain Asia program (19-HMA19-0012). Computing was supported by the resources at the NASA Center for Climate Simulation.

References

Ahmad, J. A., Forman, B. A., & Kumar, S. V. (2022). Soil moisture estimation in South Asia via assimilation of SMAP retrievals. *Hydrology and Earth System Sciences*, *26*(8), 2221–2243. https://doi.org/10.5194/hess-26-2221-2022

Beniston, M., & Stoffel, M. (2016). Rain-on-snow events, floods and climate change in the Alps: Events may increase with warming up to 4°C and decrease thereafter. *The Science of the Total Environment*, *571*, 228–236. https://doi.org/10.1016/j.scitotenv.2016.07.146

Bieniek, P. A., Bhatt, U. S., Walsh, J. E., Lader, R., Griffith, B., Roach, J. K., & Thoman, R. L. (2018). Assessment of Alaska rain-on-snow events using dynamical downscaling. *Journal of Applied Meteorology and Climatology*, *57*(8), 1847–1863. https://doi.org/10.1175/JAMC-D-17-0276.1

Blöschl, G., Bierkens, M. F. P., Chambel, A., Cudennec, C., Destouni, G., Fiori, A., et al. (2019). Twenty-three unsolved problems in hydrology (UPH)—A community perspective. *Hydrological Sciences Journal*, *64*(10), 1141–1158. https://doi.org/10.1080/02626667.2019.1620507

Chegwidden, O. S., Rupp, D. E., & Nijssen, B. (2020). Climate change alters flood magnitudes and mechanisms in climatically-diverse headwaters across the northwestern United States. *Environmental Research Letters*, *15*(9), 094048. https://doi.org/10.1088/1748-9326/ab986f

Clark, A. J. (2017). Generation of ensemble mean precipitation forecasts from convection-allowing ensembles. *Weather and Forecasting*, *32*(4), 1569–1583. https://doi.org/10.1175/WAF-D-16-0199.1

Cohen, J., Ye, H., & Jones, J. (2015). Trends and variability in rain-on-snow events. *Geophysical Research Letters*, *42*(17), 7115–7122. https://doi.org/10.1002/2015GL065320

Crawford, A. D., Alley, K. E., Cooke, A. M., & Serreze, M. C. (2020). Synoptic climatology of rain-on-snow events in Alaska. *Monthly Weather Review*, *148*(3), 1275–1295. https://doi.org/10.1175/MWR-D-19-0311.1

Freudiger, D., Kohn, I., Stahl, K., & Weiler, M. (2014). Large-scale analysis of changing frequencies of rain-on-snow events with flood-generation potential. *Hydrology and Earth System Sciences*, *18*(7), 2695–2709. https://doi.org/10.5194/hess-18-2695-2014

Friedl, M., & Sulla-Menashe, D. (2019). MCD12Q1 MODIS/Terra+Aqua land cover type yearly L3 global 500 m SIN grid V006 [Dataset]. NASA EOSDIS Land Processes DAAC. https://doi.org/10.5067/MODIS/MCD12Q1.006

Funk, C., Peterson, P., Landsfeld, M., Pedreros, D., Verdin, J., Shukla, S., et al. (2015). The climate hazards infrared precipitation with stations—A new environmental record for monitoring extremes. *Scientific Data*, *2*(1), 150066. https://doi.org/10.1038/sdata.2015.66

Garvelmann, J., Pohl, S., & Weiler, M. (2014). Variability of observed energy fluxes during rain-on-snow and clear sky snowmelt in a midlatitude mountain environment. *Journal of Hydrometeorology*, *15*(3), 1220–1237. https://doi.org/10.1175/JHM-D-13-0187.1

Garvelmann, J., Pohl, S., & Weiler, M. (2015). Spatio-temporal controls of snowmelt and runoff generation during rain-on-snow events in a mid-latitude mountain catchment. *Hydrological Processes*, *29*(17), 3649–3664. https://doi.org/10.1002/hyp.10460

Ghiggi, G., Humphrey, V., Seneviratne, S. I., & Gudmundsson, L. (2021). G-RUN ENSEMBLE: A multi-forcing observation-based global runoff reanalysis. *Water Resources Research*, *57*(5), e2020WR028787. https://doi.org/10.1029/2020WR028787

Groisman, P. Y., Knight, R. W., Easterling, D. R., Karl, T. R., Hegerl, G. C., & Razuvaev, V. N. (2005). Trends in intense precipitation in the climate record. *Journal of Climate*, *18*(9), 1326–1350. https://doi.org/10.1175/JCLI3339.1

Hall, D. K., Riggs, G. A., & Salomonson, V. V. (2006). MODIS/Terra snow cover 5-min L2 swath 500 m, version 5 [Dataset]. NASA National Snow and Ice Data Center DAAC. https://doi.org/10.5067/ACYTYZB9BEOS

Harr, R. D. (1981). Some characteristics and consequences of snowmelt during rainfall in western Oregon. *Journal of Hydrology*, *53*(3), 277–304. https://doi.org/10.1016/0022-1694(81)90006-8

Hersbach, H., Bell, B., Berrisford, P., Hirahara, S., Horányi, A., Muñoz-Sabater, J., et al. (2020). The ERA5 global reanalysis. *Quarterly Journal of the Royal Meteorological Society*, *146*(730), 1999–2049. https://doi.org/10.1002/qj.3803

Hock, R. (2003). Temperature index melt modelling in mountain areas. *Journal of Hydrology*, *282*(1), 104–115. https://doi.org/10.1016/S0022-1694(03)00257-9

Huffman, G. J., Bolvin, D. T., & Nelkin, E. J. (2015). Integrated multi-satellitE retrievals for GPM (IMERG) technical documentation. *NASA/GSFC Code*, *612*, 47.

Immerzeel, W. W., Van Beek, L. P. H., & Bierkens, M. F. P. (2010). Climate change will affect the Asian water towers. *Science*, *328*(5984), 1382–1385. https://doi.org/10.1126/science.1183188

ISRIC—World Soil Information. (2022). Retrieved from https://www.isric.org

Jalilov, S.-M., Keskinen, M., Varis, O., Amer, S., & Ward, F. A. (2016). Managing the water–energy–food nexus: Gains and losses from new water development in Amu Darya River Basin. *Journal of Hydrology*, *539*, 648–661. https://doi.org/10.1016/j.jhydrol.2016.05.071

Jeong, D., & Sushama, L. (2018). Rain-on-snow events over North America based on two Canadian regional climate models. *Climate Dynamics*, *50*(1), 303–316. https://doi.org/10.1007/s00382-017-3609-x

Jordan, R. E. (1991). A one-dimensional temperature model for a snow cover: Technical documentation for SNTHERM.89. In *This digital resource was created from scans of the print resource*. Retrieved from https://erdc-library.erdc.dren.mil/jspui/handle/11681/11677

Kendall, M. G. (1948). *Rank correlation methods*. Griffin.

Kirschbaum, D., Kapnick, S. B., Stanley, T., & Pascale, S. (2020). Changes in extreme precipitation and landslides over High Mountain Asia. *Geophysical Research Letters*, *47*(4), e2019GL085347. https://doi.org/10.1029/2019GL085347

Kraaijenbrink, P. D. A., Stigter, E. E., Yao, T., & Immerzeel, W. W. (2021). Climate change decisive for Asia's snow meltwater supply. *Nature Climate Change*, *11*(7), 591–597. https://doi.org/10.1038/s41558-021-01074-x

Kumar, S. V., Jasinski, M., Mocko, D. M., Rodell, M., Borak, J., Li, B., et al. (2019). NCA-LDAS land analysis: Development and performance of a multisensor, multivariate land data assimilation system for the national climate assessment. *Journal of Hydrometeorology*, *20*(8), 1571–1593. https://doi.org/10.1175/JHM-D-17-0125.1

Kumar, S. V., Peters-Lidard, C. D., Mocko, D., Reichle, R., Liu, Y., Arsenault, K. R., et al. (2014). Assimilation of remotely sensed soil moisture and snow depth retrievals for drought estimation. *Journal of Hydrometeorology*, *15*(6), 2446–2469. https://doi.org/10.1175/JHM-D-13-0132.1

Kumar, S. V., Peters-Lidard, C. D., Tian, Y., Houser, P. R., Geiger, J., Olden, S., et al. (2006). Land information system: An interoperable framework for high resolution land surface modeling. *Environmental Modelling & Software*, *21*(10), 1402–1415. https://doi.org/10.1016/j.envsoft.2005.07.004

Lahmers, T. M., Kumar, S. V., Rosen, D., Dugger, A., Gochis, D. J., Santanello, J. A., et al. (2022). Assimilation of NASA's airborne snow observatory snow measurements for improved hydrological modeling: A case study enabled by the coupled LIS/WRF-hydro system. *Water Resources Research*, *58*(3), e2021WR029867. https://doi.org/10.1029/2021WR029867

Lalande, M., Ménégoz, M., Krinner, G., Naegeli, K., & Wunderle, S. (2021). Climate change in the High Mountain Asia in CMIP6. *Earth System Dynamics*, *12*(4), 1061–1098. https://doi.org/10.5194/esd-12-1061-2021

Leathers, D. J., Kiuck, D. R., & Kroczynski, S. (1998). The severe flooding event of January 1996 across north-central Pennsylvania. *Bulletin of the American Meteorological Society*, *79*(5), 785–798. https://doi.org/10.1175/1520-0477(1998)079<0785:TSFEOJ>2.0.CO;2

Li, D., Lettenmaier, D. P., Margulis, S. A., & Andreadis, K. (2019). The role of rain-on-snow in flooding over the conterminous United States. *Water Resources Research*, *55*(11), 8492–8513. https://doi.org/10.1029/2019WR024950

Li, Y., Chen, Y., Wang, F., He, Y., & Li, Z. (2020). Evaluation and projection of snowfall changes in High Mountain Asia based on NASA's NEX-GDDP high-resolution daily downscaled dataset. *Environmental Research Letters*, *15*(10), 104040. https://doi.org/10.1088/1748-9326/aba926

Liu, J., Wu, Y., & Gao, X. (2021). Increase in occurrence of large glacier-related landslides in the high mountains of Asia. *Scientific Reports*, *11*(1), 1635. https://doi.org/10.1038/s41598-021-81212-9

Liu, Y., Peters-Lidard, C. D., Kumar, S., Foster, J. L., Shaw, M., Tian, Y., & Fall, G. M. (2013). Assimilating satellite-based snow depth and snow cover products for improving snow predictions in Alaska. *Advances in Water Resources*, *54*, 208–227. https://doi.org/10.1016/j.advwatres.2013.02.005

López-Moreno, J. I., Pomeroy, J. W., Morán-Tejeda, E., Revuelto, J., Navarro-Serrano, F. M., Vidaller, I., & Alonso-González, E. (2021). Changes in the frequency of global high mountain rain-on-snow events due to climate warming. *Environmental Research Letters*, *16*(9), 094021. https://doi.org/10.1088/1748-9326/ac0dde

Loukas, A., Vasiliades, L., & Dalezios, N. R. (2000). Flood producing mechanisms identification in southern British Columbia, Canada. *Journal of Hydrology*, *227*(1), 218–235. https://doi.org/10.1016/S0022-1694(99)00182-1

Maina, F. Z., Kumar, S. V., Albergel, C., & Mahanama, S. P. (2022). Warming, increase in precipitation, and irrigation enhance greening in High Mountain Asia. *Communications Earth & Environment*, *3*(1), 1–8. https://doi.org/10.1038/s43247-022-00374-0

Maina, F. Z., Kumar, S. V., Dollan, I. J., & Maggioni, V. (2022). Development and evaluation of ensemble consensus precipitation estimates over High Mountain Asia. *Journal of Hydrometeorology*, *1*(9), 1469–1486. https://doi.org/10.1175/JHM-D-21-0196.1

Mann, H. B. (1945). Nonparametric tests against trend. *Econometrica*, *13*(3), 245–259. https://doi.org/10.2307/1907187

Marks, D., Kimball, J., Tingey, D., & Link, T. (1998). The sensitivity of snowmelt processes to climate conditions and forest cover during rain-on-snow: A case study of the 1996 Pacific northwest flood. *Hydrological Processes*, *12*(10–11), 1569–1587. https://doi.org/10.1002/(SICI)1099-1085(199808/09)12:10/11<1569::AID-HYP682>3.0.CO;2-L

Mazurkiewicz, A. B., Callery, D. G., & McDonnell, J. J. (2008). Assessing the controls of the snow energy balance and water available for runoff in a rain-on-snow environment. *Journal of Hydrology*, *354*(1), 1–14. https://doi.org/10.1016/j.jhydrol.2007.12.027

McCabe, G. J., Clark, M. P., & Hay, L. E. (2007). Rain-on-Snow events in the Western United States. *Bulletin of the American Meteorological Society*, *88*(3), 319–328. https://doi.org/10.1175/BAMS-88-3-319

Merz, R., & Blöschl, G. (2003). A process typology of regional floods. *Water Resources Research*, *39*(12), 1340. https://doi.org/10.1029/2002WR001952

Morán-Tejeda, E., López-Moreno, J. I., Stoffel, M., & Beniston, M. (2016). Rain-on-snow events in Switzerland: Recent observations and projections for the 21st century. *Climate Research*, *71*(2), 111–125. https://doi.org/10.3354/cr01435

Musselman, K. N., Lehner, F., Ikeda, K., Clark, M. P., Prein, A. F., Liu, C., et al. (2018). Projected increases and shifts in rain-on-snow flood risk over western North America. *Nature Climate Change*, *8*(9), 808–812. https://doi.org/10.1038/s41558-018-0236-4

Nguyen, P., Thorstensen, A., Sorooshian, S., Hsu, K., Aghakouchak, A., Ashouri, H., et al. (2018). Global precipitation trends across spatial scales using satellite observations. *Bulletin of the American Meteorological Society*, *99*(4), 689–697. https://doi.org/10.1175/BAMS-D-17-0065.1

Nied, M., Pardowitz, T., Nissen, K., Ulbrich, U., Hundecha, Y., & Merz, B. (2014). On the relationship between hydro-meteorological patterns and flood types. *Journal of Hydrology*, *519*, 3249–3262. https://doi.org/10.1016/j.jhydrol.2014.09.089

Niu, G.-Y., Yang, Z.-L., Mitchell, K. E., Chen, F., Ek, M. B., Barlage, M., et al. (2011). The community Noah land surface model with multiparameterization options (Noah-MP): 1. Model description and evaluation with local-scale measurements. *Journal of Geophysical Research*, *116*(D12), D12109. https://doi.org/10.1029/2010JD015139

Ohba, M., & Kawase, H. (2020). Rain-on-Snow events in Japan as projected by a large ensemble of regional climate simulations. *Climate Dynamics*, *55*(9), 2785–2800. https://doi.org/10.1007/s00382-020-05419-8

Palazzi, E., Von Hardenberg, J., & Provenzale, A. (2013). Precipitation in the Hindu-Kush Karakoram Himalaya: Observations and future scenarios. *Journal of Geophysical Research: Atmospheres*, *118*(1), 85–100. https://doi.org/10.1029/2012JD018697

Pall, P., Tallaksen, L. M., & Stordal, F. (2019). A climatology of rain-on-snow events for Norway. *Journal of Climate*, *32*(20), 6995–7016. https://doi.org/10.1175/JCLI-D-18-0529.1

Pohl, S., Marsh, P., & Liston, G. E. (2006). Spatial-temporal variability in turbulent fluxes during spring snowmelt. *Arctic Antarctic and Alpine Research*, *38*(1), 136–146. https://doi.org/10.1657/1523-0430(2006)038[0136:SVITFD]2.0.CO;2

Pradhanang, S. M., Frei, A., Zion, M., Schneiderman, E. M., Steenhuis, T. S., & Pierson, D. (2013). Rain-on-snow runoff events in New York. *Hydrological Processes*, *27*(21), 3035–3049. https://doi.org/10.1002/hyp.9864

Pritchard, H. D. (2019). Asia's shrinking glaciers protect large populations from drought stress. *Nature*, *569*(7758), 649–654. https://doi.org/10.1038/s41586-019-1240-1

Putkonen, J., Grenfell, T. C., Rennert, K., Bitz, C., Jacobson, P., & Russell, D. (2009). Rain on snow: Little understood Killer in the North. *Eos, Transactions American Geophysical Union*, *90*(26), 221–222. https://doi.org/10.1029/2009EO260002

Putkonen, J., & Roe, G. (2003). Rain-on-snow events impact soil temperatures and affect ungulate survival. *Geophysical Research Letters*, *30*(4), 1188. https://doi.org/10.1029/2002GL016326

Qiu, J. (2008). China: The third pole. *Nature*, *454*(7203), 393–396. https://doi.org/10.1038/454393a

Reichle, R. H., & Koster, R. D. (2003). Assessing the impact of horizontal error correlations in background fields on soil moisture estimation. *Journal of Hydrometeorology*, *4*(6), 1229–1242. https://doi.org/10.1175/1525-7541(2003)004<1229:ATIOHE>2.0.CO;2

Reichle, R. H., Kumar, S. V., Mahanama, S. P. P., Koster, R. D., & Liu, Q. (2010). Assimilation of satellite-derived skin temperature observations into land surface models. *Journal of Hydrometeorology*, *11*(5), 1103–1122. https://doi.org/10.1175/2010JHM1262.1

Reichle, R. H., McLaughlin, D. B., & Entekhabi, D. (2002). Hydrologic data assimilation with the ensemble Kalman filter. *Monthly Weather Review*, *130*(1), 103–114. https://doi.org/10.1175/1520-0493(2002)130<0103:HDAWTE>2.0.CO;2

Rennert, K. J., Roe, G., Putkonen, J., & Bitz, C. M. (2009). Soil thermal and ecological impacts of rain on snow events in the circumpolar Arctic. *Journal of Climate*, *22*(9), 2302–2315. https://doi.org/10.1175/2008JCLI2117.1

Rodell, M., Velicogna, I., & Famiglietti, J. S. (2009). Satellite-based estimates of groundwater depletion in India. *Nature*, *460*(7258), 999–1002. https://doi.org/10.1038/nature08238

Rössler, O., Froidevaux, P., Börst, U., Rickli, R., Martius, O., & Weingartner, R. (2014). Retrospective analysis of a nonforecasted rain-on-snow flood in the alps—A matter of model limitations or unpredictable nature? *Hydrology and Earth System Sciences*, *18*(6), 2265–2285. https://doi.org/10.5194/hess-18-2265-2014

Salmon, J. M., Friedl, M. A., Frolking, S., Wisser, D., & Douglas, E. M. (2015). Global rain-fed, irrigated, and paddy croplands: A new high resolution map derived from remote sensing, crop inventories and climate data. *International Journal of Applied Earth Observation and Geoinformation*, *38*, 321–334. https://doi.org/10.1016/j.jag.2015.01.014

Sarangi, C., Qian, Y., Rittger, K., Ruby Leung, L., Chand, D., Bormann, K. J., & Painter, T. H. (2020). Dust dominates high-altitude snow darkening and melt over high-mountain Asia. *Nature Climate Change*, *10*(11), 1045–1051. https://doi.org/10.1038/s41558-020-00909-3

Singh, P., Spitzbart, G., Hübl, H., & Weinmeister, H. W. (1997). Hydrological response of snowpack under rain-on-snow events: A field study. *Journal of Hydrology*, *202*(1), 1–20. https://doi.org/10.1016/S0022-1694(97)00004-8

Slater, A. G., & Clark, M. P. (2006). Snow data assimilation via an ensemble Kalman filter. *Journal of Hydrometeorology*, *7*(3), 478–493. https://doi.org/10.1175/JHM505.1

Smith, T., & Bookhagen, B. (2018). Changes in seasonal snow water equivalent distribution in High Mountain Asia (1987 to 2009). *Science Advances*, *4*(1), e1701550. https://doi.org/10.1126/sciadv.1701550

Stimberis, J., & Rubin, C. M. (2011). Glide avalanche response to an extreme rain-on-snow event, Snoqualmie Pass, Washington, USA. *Journal of Glaciology*, *57*(203), 468–474. https://doi.org/10.3189/002214311796905686

Sui, J., & Koehler, G. (2001). Rain-on-snow induced flood events in Southern Germany. *Journal of Hydrology*, *252*(1), 205–220. https://doi.org/10.1016/S0022-1694(01)00460-7

Surfleet, C. G., & Tullos, D. (2013). Variability in effect of climate change on rain-on-snow peak flow events in a temperate climate. *Journal of Hydrology*, *479*, 24–34. https://doi.org/10.1016/j.jhydrol.2012.11.021

Tarasova, L., Basso, S., & Merz, R. (2020). Transformation of generation processes from small runoff events to large floods. *Geophysical Research Letters*, *47*(22), e2020GL090547. https://doi.org/10.1029/2020GL090547

Trubilowicz, J. W., & Moore, R. D. (2017). Quantifying the role of the snowpack in generating water available for run-off during rain-on-snow events from snow pillow records. *Hydrological Processes*, *31*(23), 4136–4150. https://doi.org/10.1002/hyp.11310

Ulbrich, U., & Fink, A. (1995). The January 1995 flood in Germany: Meteorological versus hydrological causes. *Physics and Chemistry of the Earth*, *20*(5), 439–444. https://doi.org/10.1016/S0079-1946(96)00002-X

Viviroli, D., Dürr, H. H., Messerli, B., Meybeck, M., & Weingartner, R. (2007). Mountains of the world, water towers for humanity: Typology, mapping, and global significance. *Water Resources Research*, *43*(7), W07447. https://doi.org/10.1029/2006WR005653

Wayand, N. E., Lundquist, J. D., & Clark, M. P. (2015). Modeling the influence of hypsometry, vegetation, and storm energy on snowmelt contributions to basins during rain-on-snow floods. *Water Resources Research*, *51*(10), 8551–8569. https://doi.org/10.1002/2014WR016576

Westermann, S., Boike, J., Langer, M., Schuler, T. V., & Etzelmüller, B. (2011). Modeling the impact of wintertime rain events on the thermal regime of permafrost. *The Cryosphere*, *5*(4), 945–959. https://doi.org/10.5194/tc-5-945-2011

Whitaker, A. C., & Sugiyama, H. (2005). Seasonal snowpack dynamics and runoff in a cool temperate forest: Lysimeter experiment in Niigata, Japan. *Hydrological Processes*, *19*(20), 4179–4200. https://doi.org/10.1002/hyp.6059

White, C. J., Tanton, T. W., & Rycroft, D. W. (2014). The impact of climate change on the water resources of the Amu Darya basin in central Asia. *Water Resources Management*, *28*(15), 5267–5281. https://doi.org/10.1007/s11269-014-0716-x

Würzer, S., Jonas, T., Wever, N., & Lehning, M. (2016). Influence of initial snowpack properties on runoff formation during rain-on-snow events. *Journal of Hydrometeorology*, *17*(6), 1801–1815. https://doi.org/10.1175/JHM-D-15-0181.1

Xue, Y., Houser, P. R., Maggioni, V., Mei, Y., Kumar, S. V., & Yoon, Y. (2019). Assimilation of satellite-based snow cover and freeze/thaw observations over High Mountain Asia. *Frontiers of Earth Science*, *7*, 115. https://doi.org/10.3389/feart.2019.00115

Xue, Y., Houser, P. R., Maggioni, V., Mei, Y., Kumar, S. V., & Yoon, Y. (2022). Evaluation of High Mountain Asia-land data assimilation system (version 1) from 2003 to 2016: 2. The impact of assimilating satellite-based snow cover and freeze/thaw observations into a land surface model. *Journal of Geophysical Research: Atmospheres*, *127*(7), e2021JD035992. https://doi.org/10.1029/2021JD035992

Yamazaki, D., Ikeshima, D., Tawatari, R., Yamaguchi, T., O'Loughlin, F., Neal, J. C., et al. (2017). A high-accuracy map of global terrain elevations. *Geophysical Research Letters*, *44*(11), 5844–5853. https://doi.org/10.1002/2017GL072874

Yang, T., Li, Q., Hamdi, R., Chen, X., Zou, Q., Cui, F., et al. (2022). Trends and spatial variations of rain-on-snow events over the high Mountain Asia. *Journal of Hydrology*, *614*, 128593. https://doi.org/10.1016/j.jhydrol.2022.128593

Ye, H., Yang, D., & Robinson, D. (2008). Winter rain on snow and its association with air temperature in northern Eurasia. *Hydrological Processes*, *22*(15), 2728–2736. https://doi.org/10.1002/hyp.7094

Yoon, Y., Kumar, S. V., Forman, B. A., Zaitchik, B. F., Kwon, Y., Qian, Y., et al. (2019). Evaluating the uncertainty of terrestrial water budget components over High Mountain Asia. *Frontiers of Earth Science*, *7*, 115. https://doi.org/10.3389/feart.2019.00120

You, Q., Min, J., Zhang, W., Pepin, N., & Kang, S. (2015). Comparison of multiple datasets with gridded precipitation observations over the Tibetan Plateau. *Climate Dynamics*, *45*(3), 791–806. https://doi.org/10.1007/s00382-014-2310-6

Yue, S., Pilon, P., & Cavadias, G. (2002). Power of the Mann–Kendall and Spearman's rho tests for detecting monotonic trends in hydrological series. *Journal of Hydrology*, *259*(1), 254–271. https://doi.org/10.1016/S0022-1694(01)00594-7